

Systematic Screening, Rational Development, and Initial Optimization of Efficacious RNA Silencing Agents for Human Rod Opsin Therapeutics

Edwin H. Yau^{1,2,*}, Robert T. Taggart², Mohammed Zuber^{3,†}, Alexandria J. Trujillo^{1,2}, Zahra S. Fayazi², Mark C. Butler^{2,3,‡}, Lowell G. Sheflin¹, Jennifer B. Breen^{2,§}, Dian Yu^{2,¶}, and Jack M. Sullivan¹⁻⁷

¹ Department of Pharmacology/Toxicology, University at Buffalo-SUNY, Buffalo, NY, USA

² Department of Ophthalmology (Ross Eye Institute), University at Buffalo-SUNY, Buffalo, NY, USA

³ Research Service, VA Western New York Healthcare System, Buffalo, NY, USA

⁴ Department of Physiology/Biophysics, University at Buffalo-SUNY, Buffalo, NY, USA

⁵ Neuroscience Program, University at Buffalo-SUNY, Buffalo, NY, USA

⁶ SUNY Eye Institute, Albany, NY, USA

⁷ RNA Institute at University at Albany-SUNY, Albany, NY, USA

* Current affiliation: Department of Medicine, Department of Cancer Genetics and Genomics, Roswell Park Cancer Institute, Buffalo, NY, USA

† Current affiliation: Biologist, Office of Pesticide Programs, Environmental Protection Agency, Arlington, VA, USA

‡ Current affiliation: Custom CoLABorators, Buffalo, NY, USA

§ Current affiliation: Research Analyst II, Athenex, Buffalo, NY, USA

¶ Current affiliation: Washington National Eye Center, Medstar Georgetown University Hospital/Medstar Washington Hospital, Washington, DC, USA

Correspondence: Jack M. Sullivan, Department of Ophthalmology, University at Buffalo-SUNY, Veterans Administration Western New York Healthcare System, Building 20, Room 245, 3495 Bailey Ave, Buffalo, NY 14215, USA. e-mail: jackmsullivanmdphd@yahoo.com

Received: 12 February 2019

Accepted: 15 July 2019

Published: 12 December 2019

Keywords: retinal degeneration; macular degeneration; gene therapy; high throughput screening; ribozyme; siRNA; shRNA; DNAzyme

Citation: Yau EH, Taggart RT, Zuber M, Trujillo AJ, Fayazi ZS, Butler MC, Sheflin LG, Breen JB, Yu D, Sullivan JM. Systematic screening, rational development, and initial optimization of efficacious rna silencing agents for human rod opsin therapeutics. *Trans Vis Sci Tech.* 2019;8(6):28, <https://doi.org/10.1167/tvst.8.6.28>

Copyright 2019 The Authors

Purpose: To systematically evaluate human rod opsin (*hRHO*) mRNA for potential target sites sensitive to posttranscriptional gene silencing (PTGS) by hammerhead ribozyme (hhRz) or RNA interference (RNAi) in human cells. To develop a comprehensive strategy to identify and optimize lead candidate agents for PTGS gene therapeutics.

Methods: In multidisciplinary RNA drug discovery, computational mRNA accessibility and in vitro experimental methods using reverse transcription-polymerase chain reaction (RT-PCR) were used to map accessibility in full-length *hRHO* transcripts. HhRzs targeted predicted accessible and inaccessible sites and were screened for cellular knockdown using a bicistronic reporter construct. Lead hhRz and RNAi PTGS agents were rationally optimized for target knockdown in human cells.

Results: Systematic screening of *hRHO* mRNA targeting agents resulted in lead candidate identification of a novel hhRz embedded in an RNA scaffold. Rational optimization strategies identified a minimal 725 hhRz as the most active agent. Recently identified tertiary accessory elements did not enhance activity. A 725-short-hairpin RNA (shRNA) agent exerts log-order knockdown. Silent modulation of the 725-hhRz target site in *hRHO* mRNA resulted in resistance to knockdown.

Conclusions: Combining rational RNA drug design with cell-based screening allowed rapid identification of lead agents targeting *hRHO*. Optimization strategies identified the agent with highest intracellular activity. These agents have therapeutic potential in a mutation-independent strategy for adRP, or other degenerations where *hRHO* is a target. This approach can be broadly applied to any validated target mRNA, regardless of the disease.

Translational Relevance: This work establishes a platform approach to develop RNA biologicals for the treatment of human disease.

Introduction

The sequence-specific knockdown of target disease mRNAs through posttranscriptional gene silencing (PTGS) agents offers attractive therapeutic strategies for the treatment of autosomal dominant (ad) hereditary retinal diseases. A mutation-independent (MI) approach has gained favor in gene therapy strategies using a PTGS agent, which suppresses the endogenous expression of both the wild-type (WT) and the mutation-containing transcripts, which is combined with an expression construct that produces a WT transcript that is unaffected by the specific gene silencing agent.¹⁻⁹ This approach addresses the profound genotypic heterogeneity that exists for many ad retinal degenerations. As any mRNA target has extensive and dense secondary and tertiary structure, and because random human mutation will most often result in mRNA changes that are inaccessible to binding of an RNA therapeutic, the MI approach offers strong rationale for the further development of RNA drugs. In ad hereditary diseases many different mutations in the same gene (genotypic variability) can result in the same or different phenotypes with a wide range of clinical anatomic presentation or kinetics of emergence (phenotypic variability). Developing specific therapeutic agents for each mutation would be exceedingly cumbersome, expensive, and therefore prohibitive as a general strategy for human clinical translation. The MI approach, also called by us the “knockdown-reconstitute” (KD-RECON) approach, involves the knockdown of both intrinsic WT and mutant target mRNAs using a single PTGS agent paired with the simultaneous reconstitution of WT protein expression through an engineered mRNA construct that is resistant to cleavage by the specific PTGS agent. The reconstitution of WT target protein expression prevents expected deleterious haploinsufficiency for the target cell that is treated. There has been substantial effort in applying the MI approach toward therapy for ad retinitis pigmentosa (adRP) caused by mutations in *RHO* mRNA using both ribozyme and RNA interference (RNAi) technologies.⁶⁻⁸ As therapeutic rescue in mouse models has only been partial, there remains need for more effective agents, or variants of the MI strategy that prove more broadly effective prior to clinical translation.

We take a bioengineering, biophysical, and biochemical approach toward developing a MI gene therapy for the treatment of model human rod opsin

(*hRHO*)-associated adRP. We sought to systematically analyze and optimize PTGS agents targeting *hRHO* mRNA. The major limiting factor in the success of PTGS agents is the difficulty in identifying target mRNA regions that are sensitive to PTGS agents in a cellular environment. Sensitivity to knockdown by PTGS agents varies greatly along any given target mRNA. Regardless of PTGS technology, most mRNA target regions are highly resistant to PTGS annealing/knockdown due to dense stable secondary structure, overriding tertiary structure, dynamic protein coating, and distributed lifetimes in different environments in the cell.¹⁰⁻¹⁵ We have shown that the first major challenge or bottleneck in PTGS development is to identify regions that are accessible.¹⁶ We recently reported on a high-throughput screening (HTS) methodologic approach to identify a lead candidate PTGS agent to an arbitrary mRNA target.¹⁷ Here, we describe the identification of a lead candidate agent to *hRHO* mRNA and our initial efforts toward rational optimization.

Our PTGS technological modality is focused on use of hammerhead ribozyme (hhRz), which are small RNA sequences capable of enzymatic cleavage of another target RNA independent of host cell machinery. Originally discovered as self-cleaving in cis (intramolecular) sequences in self-replicating plant viroid RNAs, hhRz consist of three helices surrounding a conserved 11-nucleotide (nt) catalytic core sequence that folds into an RNA enzyme. They cleave RNA sequences at ‘NUH’ sites (N = any nucleotide, H = any nucleotide, excluding G). Trans-cleaving hhRzs can be constructed by separating the strands of two of the helices to form single-stranded arms that embrace the enzyme core, and designing these arms to be antisense complementary to an accessible region of a specific target mRNA. Upon collision with and annealing to the target, the nascent hhRz:substrate hybrid forms, conformational changes occur in the hhRz and substrate that position critical nts for in-line Sn2 endonucleolytic attack, and enzymatic cleavage proceeds at the specific target nt, which requires an NUH↓ cleavage site.¹⁸⁻²¹ If the two cleavage products are readily released the hhRz has the capacity for enzymatic turnover of multiple copies of target mRNA.

In addition to ribozymes, we also evaluated PTGS using RNAi, which involves an evolutionarily conserved phenomenon where double-stranded RNA mediates the sequence-specific cleavage of target RNA using host cellular machinery. In mammalian

cells, RNAi is generally triggered by 19- to 21-nt RNA duplexes with symmetric 2-nt 3' overhangs and 5'-phosphate termini, called small interfering RNA (siRNA). These siRNA duplexes can be processed from short-hairpin RNA (shRNA) precursors by the cytoplasmic ribonuclease-III enzyme, called Dicer. A multiprotein complex known as the RNA-inducing silencing complex (RISC) then associates with these duplexes, energetically selects the guide strand from the duplex, and uses the bound guide to identify complementary regions prior to cleavage of the target mRNA.^{22–24} Here, the actual cleavage event occurs by way of protein-dependent catalysis (Ago2).

In this study, we sought to systematically evaluate the model *hRHO* mRNA target to determine the best site(s) for development of hhRz or shRNA PTGS agents and to initiate optimization of these agents toward MI gene therapy. *hRHO* mRNA is an excellent target because the many pathogenic mutations in this gene (>200) constitute 25% to 30% of all adRP in the United States.^{25–28} It is also a relatively abundant mRNA target. And, it is a challenging target because its mRNA and protein are very stable. Extensive target mRNA structures limit accessibility to collision, seeding, and full binding of any PTGS agent (antisense, ribozyme, RNAi). Because there is no reliable way to completely predict the successful targeting of a disease mRNA using PTGS agents, there is a need to test PTGS agents against precise replicas of human mRNA disease targets. Development of PTGS agents designed against animal mRNAs may not provide optimal agents for human mRNA targets because codon degeneracy and divergence in 5'- and 3'-untranslated regions lead to different mRNA folding patterns and accessibility, even for mRNAs encoding highly homologous proteins such as rhodopsin where PTGS attack sites may be identical (Trujillo et al., unpublished material). PTGS efficacy demonstrated against an animal model mRNA does not obligate equivalent performance against the human target.

In human cell culture, a human mRNA target can be expressed, with identical primary sequence as occurs in vivo and which predisposes for the range of conformational structures that a PTGS agent would encounter in a human gene therapy. PTGS silencing occurs in the housekeeping sector of cellular functionality. Successful tests of knockdown efficacy against a human target mRNA expressed in cultured cells have predictive value for gene therapy outcomes because a PTGS agent has faced most, if not all, of the same biophysical variables for molecular recogni-

tion and cleavage of the same target that it will encounter in photoreceptors or target cells of patients.

Materials and Methods

Computational Analysis of Human Rod Opsin mRNA Accessibility

The human rod opsin mRNA construct (*hRHO*; GenBank: NM_000539.3)²⁹ is the full-length mature transcript of rod photoreceptors and begins from transcription start and extends to 21 nt downstream of the initial (dominant) polyadenylation signal (1506–1511) in the vicinity of the cleavage site where unstructured polyadenylation would occur. The secondary structure of the full-length *hRHO* mRNA transcript was analyzed for local folding regions with highly probable and stable secondary structures with substantial (≥ 8 nt) single-stranded regions. We employed three contemporary algorithms (MFold, SFold, OligoWalk [OW])^{30–32} to predict accessible regions in human *RHO* mRNA in an established approach developed in this lab, multiparameter prediction of RNA accessibility (mppRNA).^{14–17,28} A three-dimensional (3D) RNA structure over limited regions can be reliably estimated from a publicly available algorithm called RNA Composer³³ (in the public domain, <http://rnacomposer.cs.put.poznan.pl>); this algorithm draws on published RNA structured elements from the Protein Data Base (repository also for RNA crystal structures).

Gene-Specific mRNA Accessibility Site Tagging (gsMAST)

We adapted a method, mRNA accessibility site tagging (MAST),³⁴ for use with *hRHO* mRNA target to conduct experimental accessibility mapping. We reduced the complexity of the published MAST procedure, which uses fully randomized combinatorial probes that did not work in our hands, to a gene-specific MAST (gsMAST), which was effective at testing explicit accessibility to annealing of an ensemble of discrete *hRHO*-specific antisense primers. *hRHO*-specific oligodeoxynucleotide (ODN) MAST tags (18 nt) were generated for computationally determined accessible and inaccessible regions. MAST tags were competitively hybridized to in vitro transcribed full-length *hRHO* mRNA attached to magnetic beads. Linearized full-length *hRHO* plasmid template (2 μ g) was transcribed by T7 RNA polymerase in a 40- μ L reaction according to manu-

facturer's specifications (Ambion MEGAscript T7 kit; Ambion, Austin, TX) at 37°C for 2 to 3 hours with 7.5 mM of each NTP and 375 μM biotinylated-UTP (Enzo Life Sciences, Farmingdale, NY) to yield approximately 5% incorporation at available U sites. Plasmid DNA was digested with RNase-free DNase and unincorporated nt were removed by passage through a G50 spin column (GE Healthcare, Pittsburgh, PA). Typically, 50 to 100 μg of RNA transcript was obtained from each μg of plasmid DNA. *hRHO* mRNA with biotin-UTP incorporated was attached to Dynal M-280-streptavidin beads (Dynal; Invitrogen, Carlsbad, CA) in physiologic buffer and gsMAST Tags were added, allowed to bind, and then the beads were extensively washed with buffer. Bound tags were eluted by heating to 95°C and polymerase chain reaction (PCR) amplified using Taq DNA Polymerase. Eluted MAST tags were cloned into TOPO-TA plasmid (TOPO TA Cloning for sequencing, PCR-4 TOPO vector, 45-0030; Invitrogen) and transformed into competent *Escherichia coli* cells (GC10 cells, Gene Choice, from Genesee Scientific, El Cajon, CA), purified by standard DNA minipreps (Promega, Madison, WI), and analyzed by standard DNA sequencing.

cDNA Mapping of Accessible Ribozyme Sites (cMARS)

The 40-μL in vitro transcription reaction mixtures containing 2-μg linearized plasmid, 7.5 mM of each ribonucleotide triphosphate and T7 RNA polymerase were incubated at 37°C for 2 to 3 hours following manufacturer recommendations (MegaScript; Ambion). Plasmid DNA was digested by addition of four units of Turbo DNase (RNase free; Ambion) and incubation for 30 minutes at 37°C. The transcript reaction was fractionated on a G50 spin column containing 10 mM Tris-HCl, 140 mM NaCl (pH 7.5) and passed through a Micropure-EZ spin column (Amicon) to remove enzymes. The native RNA transcript was used directly for the cMARS protocol. Four ODN probe library sets were synthesized, terminated at the 3' end with antisense sequences corresponding to a set of hhRz cleavage sites, followed upstream by a random 6 mer, and then capped with a constant amplifiable sequence at the 5' end. In vitro, these four probe sets are specific for the 12 possible types of hhRz cleavage sites (NUH↓). Ribozyme cleavage sites accessible for hybridization with the probes initiated cDNA synthesis from that site by Superscript polymerase (ThermoFisher Scien-

tific, Imperial, PA). cDNA first-strand synthesis products were mapped by PCR amplification with a series of human opsin-specific upstream primers. PCR products were screened by nondenaturing agarose gel electrophoresis and by DNA sequencing. Details of the cMARS methodology will be presented elsewhere (unpublished material).

Vectors and Cloning

Ribozyme cDNA constructs designed against NUH↓ cleavage sites in accessible and inaccessible regions (see Table 1) were directionally ligated into the *Sal I/Pst I* sites in pNEB-VAI-hhRz-1 or pNEB-VAI-hhRz-2 vectors. pNEB-VAI-hhRz-1 and pNEB-VAI-hhRz-2 vectors were generated by cloning the gene for VAI as a *BssHIII-XbaI* fragment from pAdvantage (E1711; Promega) into pNEB193-T7 (modified by us from pNEB193 from New England Biolabs to have a T7 promoter immediately upstream of the multiple cloning site) and then making extensive further modifications.^{10,35} Modified stem-loop structures (designed using secondary structure analysis) were added as a series of adapters. Details on the construction of the pNEB-VAI-hhRz-1 plasmid, also known as pUC-VAL, was previously described.¹⁷ Details on the construction of the pNEB-VAI-hhRz-2 construct scaffold (pPrislei) are presented (Supplementary Materials). All constructs were confirmed by DNA sequencing. Because there is a strong intragenic RNA-Pol-III promoter (A, B boxes) in the VAI sequence, both in vitro transcription (with upstream T7 promoter) and in cellula transcription can occur from the same plasmid for either type of construct. Expected RNA structures of native VAI RNA and those of the two engineered VAI hhRz scaffold constructs are shown (Fig. 1).

RHO-IRES2-SEAP Vector

The plasmid was generated by PCR amplification of full-length human *RHO* cDNA and ligation into the *BglII/SalI* sites within the multiple cloning site upstream of the internal ribosome entry site (IRES) element in pIRES2-EGFP vector (Takara Bio USA (formerly known as Clontech), Mountain View, CA; EGFP is enhanced green fluorescent protein). *RHO-IRES*-secreted alkaline phosphatase (SEAP) was generated by adding an *EcoRI* site just downstream of the IRES element in *RHO-IRES2-EGFP* through a *BmgBI/BstXI* adapter, and cloning the *SEAP* gene as an *EcoRI/MfeI* fragment from pSEAP2-control vector (#631717, GenBank Accession No: U89938;

Table 1. Hammerhead Ribozyme Target Sequences

HhRz	Target Sequence in Rho mRNA
250	5'-UGGGCUUCCCCAUCA-3'
257	5'-UCCCCAUAACUUC-3'
263	5'-UCAACUUCUCACGC-3'
266	5'-ACUUCUCACGCUCU-3'
272	5'-UCACGCUCUACGUCA-3'
274	5'-ACGCUCUACGUACC-3'
309	5'-CACGCCUCUACAUA-3'
311	5'-CGCCUCUACAUA-3'
316	5'-CUAACUACAUCCUG-3'
320	5'-ACUACAUCUGCUCA-3'
326	5'-UCCUGCUAACCUAG-3'
332	5'-UCAACCUAGCCGUGG-3'
380	5'-GCACCCUCUACACCU-3'
382	5'-ACCCUCUACACCU-3'
388	5'-UACACCUCUCUGCAU-3'
390	5'-CACCUCUCUGCAUGG-3'
725	5'-UCGUGGUCCACUUA-3'
730	5'-GUCCACUACCAUC-3'
731	5'-UCCACUACCAUCC-3'
737	5'-UCACCAUCCCAUGA-3'
814	5'-CAGGAGUCAGCCACC-3'
995	5'-CCGCCAUCUACAACC-3'
1049	5'-GCAUGCUCACCACCA-3'
1058	5'-CCACCAUCUGCUGCG-3'
1197	5'-ACACCUUCCCCCAGC-3'
1362	5'-CUGGAGUCCACGUU-3'
1370	5'-CCACGUUCCCAAGG-3'
1411	5'-CCCAACUCAUCUUUC-3'
1414	5'-AACUCAUCUUUCAGG-3'
785	5'-UCACCGUCAAGGAGG-3'
485	5'-UGGUGGUCCUGGCCA-3'
525	5'-GGUGGUCCUGGC-3'
1135 (P347S)	5'-GUGGCCUCGGCCUAA-3'

Hammerhead ribozyme sequences are numbered according to their cleavage site in the dominant full-length transcript of *hRHO* mRNA. For example, HhRz 316 (CUA↓) is designed to cleave the phosphodiester bond immediately after A316. NUH↓ cleavage triplets are highlighted in bold in each target sequence. HhRzs 485 and 525 are previously characterized agents from another lab (Gorbatyuk et al.⁶). HhRz 1135 targets the CUC↓ triplet generated in the Pro347Ser rhodopsin mutant, which causes severe, early-onset adRP. The 1135 (P347S) hhRz targets a CUC↓ motif that emerges from the human P347S mutation (CCC↓ → CUC↓); note that the NUH↓ cleavage motif arises in the context of the boundary codon at A346 (347 codon is underlined and NUH is italicized).

Clontech) to replace the EGFP cDNA downstream of the IRES sequence. A construction schematic of the p*RHO*-IRES-SEAP vector is shown (Fig. 2A).

pSEAP-*cis*-hhRz Reporter Construct

The plasmid was generated by directionally cloning the *SEAP* gene as a *NheI*-*XhoI* fragment from pSEAP2-control vector into pcDNA3.1-Hygro (Invitrogen) downstream of the cytomegalovirus (CMV) promoter. An *ApaI*-*PmeI* adapter sequence was added into the 3'UTR of the *SEAP* gene after the STOP codon. Ribozyme cDNA constructs were directionally ligated into the *ApaI*/*PmeI* site. Cleavage within the 3'UTR of the SEAP mRNA is expected to shorten the lifetime of the mRNA and decrease SEAP protein production and secretion. A construction schematic of the pSEAP-*cis*-hhRz reporter vector is shown (Fig. 2B).

shRNA Expression Constructs

ShRNA cDNA constructs for RNAi expression were directionally ligated into the *BglII*/*XhoI* sites into pSUPER-Puro vector (OligoEngine, Seattle, WA).³⁶ The shRNA design and schematic are shown below with target sequences (Fig. 2C). ShRNAs are expressed from the human H1 promoter (strong extragenic RNA Pol-III).

Oligodeoxynucleotides were synthesized by Sigma GenoSys (The Woodlands, TX) or Integrated DNA Technologies (Coralville, IA).

Full-Length Human *RHO* Expression Construct

The p*RHO*-fix5UT vector contains the full-length *hRHO* cDNA encoding sequence under the transcriptional control of a CMV promoter (from the pcDNA3.1[+]-Hyg parent vector). This vector encodes the entire human *RHO* mRNA, with the entire 5'UTR sequence and the 3'UTR sequence ending 21 nt downstream of the dominant poly A site (around the site where polyA would be added). The p*RHO*-fix5UT vector was generated from a vector used in Abdelmaksoud et al.¹⁶ where the human *RHO* cDNA harvested from pCIS^{29,37} (pCIS is a CMV expression vector with a synthetic intron) was cloned downstream of the CMV promoter in pcDNA3. In this original *hRHO* expression construct, the first 74 nt of the 5'UTR was replaced with vector sequence. The p*RHO*-fix5UT vector restores the full *hRHO* 5'UTR, and allows for the cellular expression of a bona fide full-length mature human *RHO* mRNA target

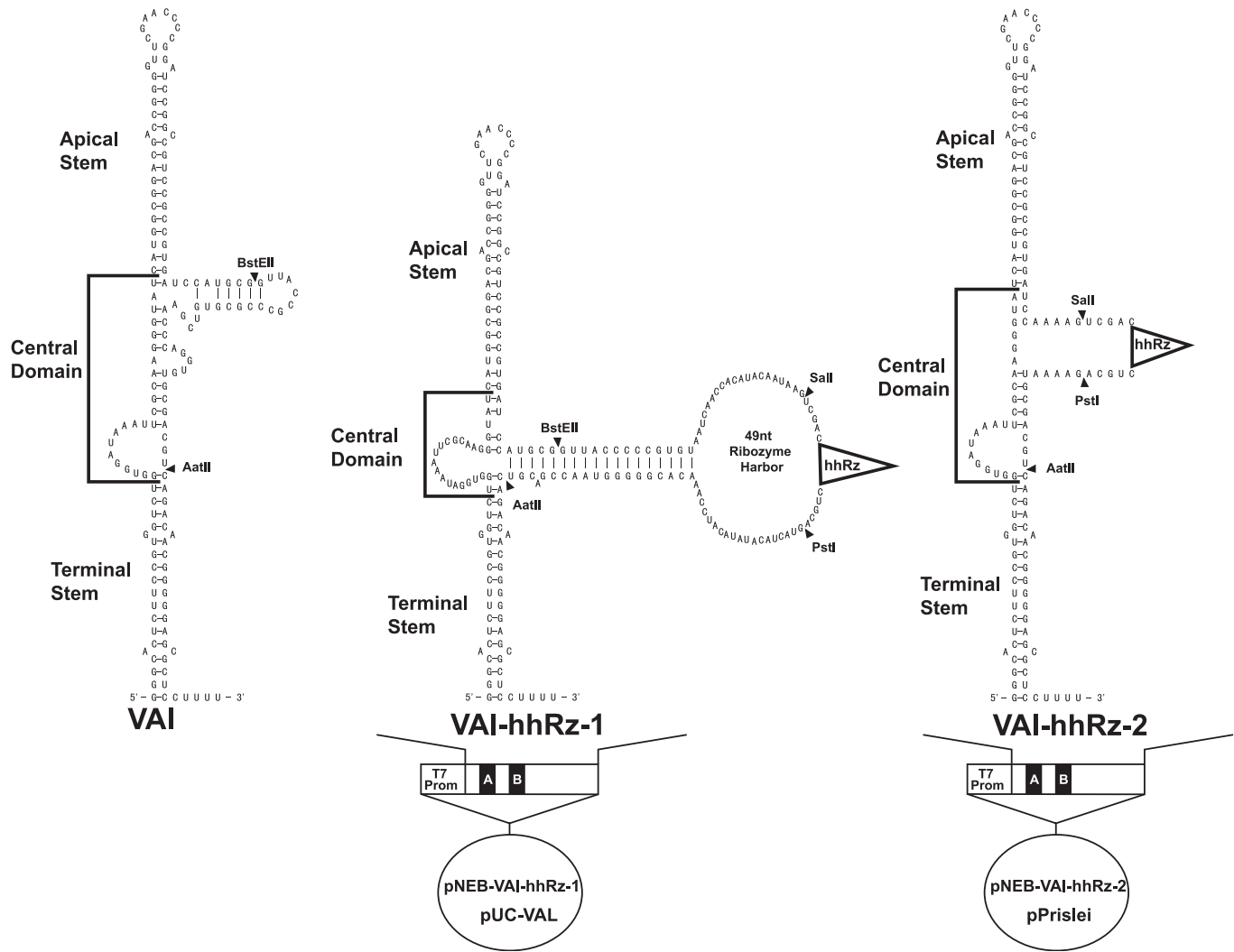


Figure 1. Predicted RNA structures of WT VAI and VAI scaffold derivatives. The most stable RNA structures for WT VAI and the scaffold RNAs expressed from the pNEB-VAI-hhRz-1 (pUC-VAL) and pNEB-VAI-hhRz-2 (pPrislei) plasmids. Plasmid designs for the two plasmids are shown beneath the scaffold RNAs.

through the first (dominant) polyA signal. This expression construct is a model for PTGS targets that model human clinical trial mRNAs.

Mutagenized Human *RHO* Expression Constructs

In vitro site-directed mutagenesis of p*RHO*-fix5-UT was carried out using the QuickChange Multi Site-Directed Mutagenesis Kit (Stratagene, San Diego, CA), where mutagenic primers containing desired mutations anneal to denatured template DNA. Mutagenic primers are then extended using high fidelity *PfuTurbo* DNA polymerase (Stratagene). A DpnI endonuclease specific for methylated DNA is used to digest parental DNA template, allowing

enrichment of mutant constructs prior to transformation into chemically competent *E. coli* and subsequent cloning and sequencing. The QuickChange Multi kit is capable of site-specific mutagenesis of one to three sites in plasmid DNA. Constructs p*RHO*-725-HARD, p*RHO*-725-731-HARD, and p*RHO*-P347S (*adRP* mutant) were generated using this kit with mutagenic primers designed according to the manufacturer's recommendations (primers were 25–45 nt in length with a melting temperature >75°C). Sequences for mutagenic primers are (mutated sites are shown in bold): p*RHO*-725-HARD (5'-TTTTGTCATCATGTTTCGTGGT**G**CACTTCACCATCCCC-3'), p*RHO*-725-731-HARD (5'-TTTTGTCATCATGTTTCGTGGT**G**CACTT**T**ACCATCCCC-3')

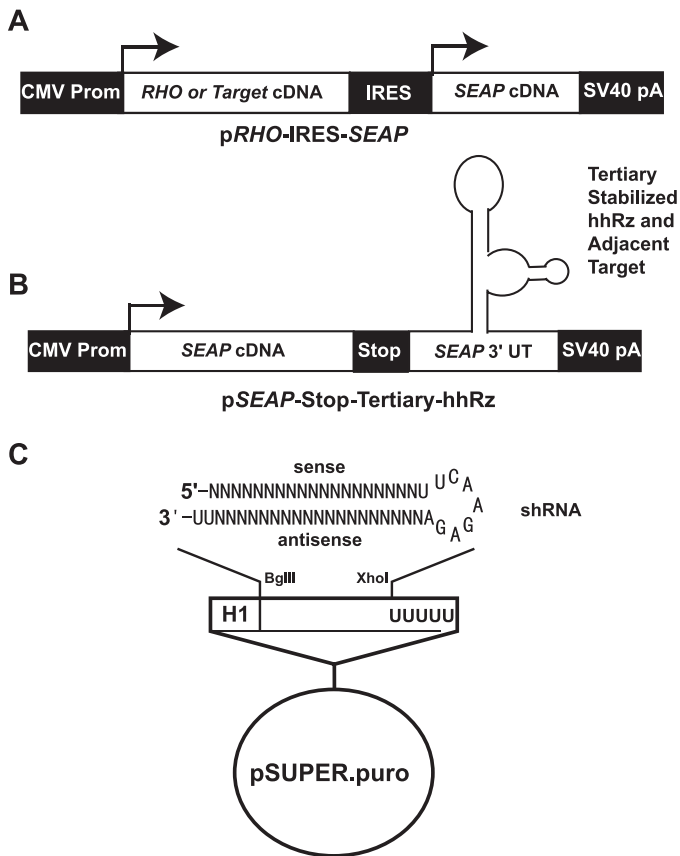


Figure 2. Expression constructs. (A) *RHO*-IRES-SEAP construct. This construct transcribes a bicistronic mRNA, which translates an *RHO* protein (cap-mediated translation) and a SEAP protein (IRES-mediated cap-independent translation). The SEAP protein is proportional to the levels of the bicistronic mRNA, is thermally stable, and is quantitatively secreted.³⁹ (B) pSEAP-*cis*-hhRz reporter construct. The hhRz is expressed in *cis* within the 3'UTR of the SEAP mRNA. When the hhRz cleaves the lifetime of the SEAP mRNA is reduced, thus suppressing translation of SEAP protein and its secretion. (C) ShRNA expression construct. The hairpin RNA is modeled after a prior study³⁶ and is transcribed by the strong human H1 promoter, an extragenic RNA Pol-III promoter.

and p*RHO*-P347S (5'-CGAGCCAGGTGGC-C \overline{C} TCGGCCTAAGACCTGC-3').

In Vitro Ribozyme Cleavage Reactions

In Vitro Transcription

Ribozyme and *hRHO* target transcription plasmids were linearized by digestion to completion with appropriate restriction enzymes immediately downstream of the functional RNA element. Templates were purified by ethanol precipitation. Linearized plasmids were mixed in a 6:1 ratio of enzyme to substrate (*hRHO*) and the MEGAShort Script T7 kit or MEGAScript T7 kit (Ambion) was used to

perform in vitro transcription of ribozyme and *hRHO* target RNAs. In co-synthesize/cleavage reactions the enzyme and target plasmid templates were transcribed at 37°C and the cleavage reaction occurred concurrently in the same reaction tube in commercial kit transcription buffer at the Mg^{2+} level present (Mg^{2+} is titrated for maximum production and is likely as large as 20 mM). Reactions were purified using the MEGAclean column (Ambion), mixed with 6× formamide-containing loading buffer, and heated to 95°C for 10 minutes. Samples were run on a denaturing 4% or 5% polyacrylamide 8.3 M urea gel at 100 mV for 45 minutes. After staining the gel with SYBR Gold Nucleic Acid Gel Stain (Invitrogen), transcription and cleavage products were visualized with 300-nm transillumination. In some experiments the hhRz and substrate RNAs were individually transcribed, cleaned, and then spectrophotometrically quantified (NanoDrop; ThermoFisher Scientific) prior to mixing for in vitro cleavage reactions. When transcription and cleavage assays were separate, the individual quantified RNAs were added independently to ribozyme reaction buffer (typically 10 mM Tris-HCl, pH 7.5) and the reaction at 37°C was initiated by addition of $MgCl_2$ (typically to 10 mM).

Cell Culture and Transfection

Suspension-adapted human embryonic kidney cells (HEK293S) were used for this study.³⁸ For screening of intracellular accessibility of target mRNAs and knockdown, HEK293S cells were engineered to stably express *phRHO*-IRES-SEAP (293S-*RHO*-IRES-SEAP).¹⁷ Extracellular secreted SEAP reporter protein activity has been shown to correlate to intracellular SEAP RNA levels,³⁹ making it an ideal reporter for PTGS screening. Cells (293S-*RHO*-IRES-SEAP, naïve HEK293S) were transiently transfected (Lipofectamine-2000; Invitrogen) in suspension according to manufacturer's suggestions. Ribozyme or shRNA plasmids were transfected into stable bicistronic expressing cells or co-transfected with *hRHO* target plasmid at a 5 µg: 333-ng ratio in 6-well dishes (15-fold mass excess of hhRz or shRNA plasmid). A human embryonic retinoblast culture line (HER224)⁴⁰ was also used to test knockdown of full-length *hRHO* expression. Both HEK293S and HER224 were transformed human cell lines and were used in this context because they can be transfected with exceptionally high efficiency using lipofectin techniques (e.g., Lipofectamine). We did not use these cells as representative of any differentiated cellular phenotype, as there is none. PTGS occurs in the space of

cellular housekeeping (steady-state mRNA levels, steady state protein levels) and for this context these cell lines are adequate vehicles for RNA drug discovery. Therapeutic PTGS performance can only be determined in vivo in appropriate animal model systems.

SEAP Assay

Conditioned cell-culture media (50 μ L) was transferred to separate wells in black-walled 96-well plates (microtest 96-well Optilux Assay plate, #353948; BD Falcon; BD Biosciences, Franklin Lakes, NJ) and incubated at 65°C for 30 minutes to inactivate heat-sensitive phosphatases. After cooling to room temp, 45 μ L of diethanolamine assay buffer (1 M diethanolamine, pH 9.8, 1 mM MgCl₂, 1 mM L-homo-arginine) was added per well, followed by 5 μ L of 4-methyl-umbelliferyl-phosphate (4-MUP) fluorescent substrate to a final concentration of 50 μ M per well. SEAP reaction was incubated at room temperature (22°C) for 1 hour before measuring fluorescence (355-nm maximum excitation/460-nm maximum emission of the fluorescent SEAP reaction product, 4-methyl-umbelliferone) on an Ascent Fluoroskan FL plate reader (355 \pm 19 nm FWHM/ 460 \pm 12 nm FWHM; ThermoFisher Scientific; FWHM is full-width half-maximum).¹⁷

Real-Time Quantitative Reverse Transcription-PCR

Total RNA was purified from transfected cell cultures 48 hours posttransfection with RNeasy plus mini kit (Qiagen, Hilden, Germany). cDNA synthesis was performed using 400 ng of total RNA with the AffinityScript Reverse Transcriptase system (Stratagene) using the supplied oligo(dT) primers. Quantitative PCR for *hRHO* was performed in a Smart Cycler II (Cepheid Inc) thermocycler. Primers that spanned adjacent exons and a probe containing a fluorescent dye (FAM) at the 5' end and a quenching dye (BHQ1) at the 3' were designed using primer quest software (Integrated DNA Technologies).¹⁷ Rhodopsin primers (5'-AATTTGGAGGGCTTCTTTGCCACC-3', 5'-AGTTGCT-CATGGGCTTACACACCA-3' with probe 5'6-FAM-AAATTGCCCTGTGGTCC-TTGGTGGT-3'BHQ1) were analyzed on plasmid DNA and genomic DNA to demonstrate their specificity and sensitivity. Human β -actin gene was used as endogenous control with the primers (5'-GTCCCCC-AACTTGAGATGTATG-3', 5'-AAGT-CAGTGACAGGTAAGCC-3' and probe 5'6-

FAM-CTGC-CTCCACCCACTCCCA-3'BHQ1). Quantitative PCR reactions were assembled by mixing equal volumes of PCR primers (0.5 μ M) and probe primer (0.25–0.5 μ M) with Amplitaq Gold PCR master mix (Applied Biosystems; ThermoFisher Scientific), dispensing into 25- μ L reaction tubes and adding 2 μ L of the first strand cDNA sample or plasmid cDNA standard. Thermocycler conditions were 94°C (6 minutes) followed by 45 cycles at 94°C (30 seconds), 58°C (15 seconds), and 72°C (30 seconds). Fluorescent intensity was measured during the 72°C extension, which showed log-linear detection of the respective cDNA over a range from 10 attograms (10 \times 10⁻¹⁸ g) to 20 pg. Standard samples were analyzed in quadruplicate and first strand cDNA samples were analyzed in duplicate or triplicate using software provided with the instrument (Smart Cycler II Thermal Cycler; Cepheid Inc, Sunnyvale, CA). See [Supplementary Materials](#) for the $\Delta\Delta$ Ct method of human RHO mRNA measurement.

Quantitative Analysis

Transfection experiments were initially subject to one-way ANOVA to evaluate the null hypothesis (no differences among all samples); criterion statistical significance level was set at $P < 0.05$. Post hoc *t*-tests were used to evaluate differences between samples and controls or between samples. The Levene test for uniformity of variance was employed to project use of parametric or nonparametric hypothesis testing. Descriptive statistics were represented as the mean \pm the standard deviation (SD) and/or the standard error of mean (SEM); note SEM is related to the SD scaled by the square root of the sample number. All analysis for basic statistics, fitting and statistical hypothesis testing was conducted in Origin (Origin Lab Corporation, Northampton, MA).

Results

Identifying Accessible Regions in Human RHO mRNA

All PTGS technologies are conditionally dependent upon a rate-limiting, second-order molecular annealing event in vivo. Because every mRNA target is folded into dense secondary structures, with overriding tertiary structures, heterogeneous and specific protein binding and expected, dynamic fluctuations, highly accessible sites that provide

platforms for PTGS annealing are rare in any mRNA target. There are a total of 236 hhRz NUH↓ cleavage sites in the dominant full-length *hRHO* mRNA (Supplementary Fig. S1). It is impractical to test efficacy for gene-based biologics at this number of sites without robotic tools. Cleavage sites are found distributed throughout the entire mRNA, as expected for a probability of NUH↓ occurrence of approximately once for every 12 nt; this allows a versatile application of the hhRz as a knockdown agent when searching for the most optimal accessible regions across any arbitrary mRNA target. Using a combination of bioinformatics and experimental approaches, we sought to systematically identify the regions in *hRHO* that are potentially accessible and then to test for target knockdown efficacy in these preselected regions relative to (control) sites in which accessibility was predicted to be low or nonexistent.

We previously established the mppRNA computational approach to search for accessible regions of a target mRNA and this led us to hhRz agents able to significantly suppress target *RHO* protein in cultured human cells.^{16,17,28} The target mRNA is folded with MFold, SFold, and RNAStructure. The output of MFold and SFold algorithms are taken as vectors that represent accessibility maps along the target mRNA. The RNAStructure output is operated upon with OW to obtain a local folding energy map along the target mRNA. The raw vector output of MFold (sscount) is normalized to the number of structures in the ensemble to yield a frequency of accessibility along the target ($0 \leq P_{MF} \leq 1$) (Fig. 3A). This is not a true probability but is biased to assessment of a range of structures in the local folding neighborhood of the (most stable) minimal free energy structure (MFE). A 15-nt averaging window is then moved along the map to filter the raw output with an antisense span comparable to that of the hhRzs being tested (15-nt total; Fig. 3A, red trace). A 15-nt window corresponds to the binding span of a symmetrical 7nt/7nt hhRz (the cleaving nt [H of NUH↓] of the substrate does not bind). A 15-nt antisense span is a reasonable starting point to identify a lead candidate agent. The SFold vector output (sstrand) represents the estimated accessibility probability along the target and is a true probability given that a Boltzmann energy algorithm has sampled the full astronomic space of the fold ($0 \leq P_{SF} \leq 1$; Fig. 3B); the number of possible structures is proportional to 4^N where N is the number of nts. Here too, a 15-nt averaging window is used to filter the raw map (Fig. 3B, green trace). The OW map has intrinsic ordinate units of free

energy (kCal/mole) and is obtained by sampling the RNAStructure folding matrix by computationally moving a 15-nt window along the target mRNA and calculating the local folding energy (LFE) within each window, which is then averaged over all structures in the ensemble. The RNAStructure raw output is also based upon identifying the MFE structure. We linearly transform the OW map into a unitless scale map by adding sufficient positive energy to each point such that all data are just greater than 0 kCal/mol and then normalize to the resultant maximum positive energy (Fig. 3C; blue trace). This output too is not a true probability, but it allows bioinformatics comparison of the output vectors because all the maps now have the same ordinate units ($0 \leq P_{MF}, P_{SF}, P_{OW} \leq 1$). Currently, we assume equivalent weights of all vector estimators, and at each nt we take the product of the raw MFold vector, the raw SFold vector, and the rescaled OW vector, to achieve a raw mppRNA map (Fig. 3D). As in the individual average maps, we filtered the global mppRNA map with a 15-nt window, which similarly shows nonuniformity of accessibility along the target (violet trace). Critically, we are searching for regions in the target mRNA, which are predicted to be accessible by all algorithms (the intersection set of accessibility by the three algorithms). All three algorithms predict a strong broad region of accessibility (~110 nt) between 653 and 763 nt (red bar).

The 15-nt window-averaged global mppRNA probability map across the entire mature human *RHO* mRNA was further analyzed to rank order the predicted accessible regions (Fig. 4A). The mean value of the access probability across the entire target was determined (0.193 ± 0.007 SEM). Positive peaks greater than the mean mppRNA value were numbered (Fig. 4A), and then computationally integrated to determine their respective weights at various sites along the transcript (Fig. 4B). The most heavily weighted region of accessibility of *hRHO* mRNA (peak 9) occurs between 653 and 763 nt (110-nt span), which is marked in the averaged global map (red bar, Fig. 4A) and in the expanded region of that map (Fig. 4C). Note that regions targeted successfully in a prior study from this lab¹⁶ also showed accessibility peaks with substantial weight (e.g., 250 peak [4] harboring 266 cleavage site; 1411 peak [21] harboring the 1411 and 1414 cleavage sites). Note that the region of the MI 485 hhRz targeting has low predicted accessibility, and the region of MD hhRz or shRNA P347S targeting (around nt 1135) is also in a region of low accessibility.

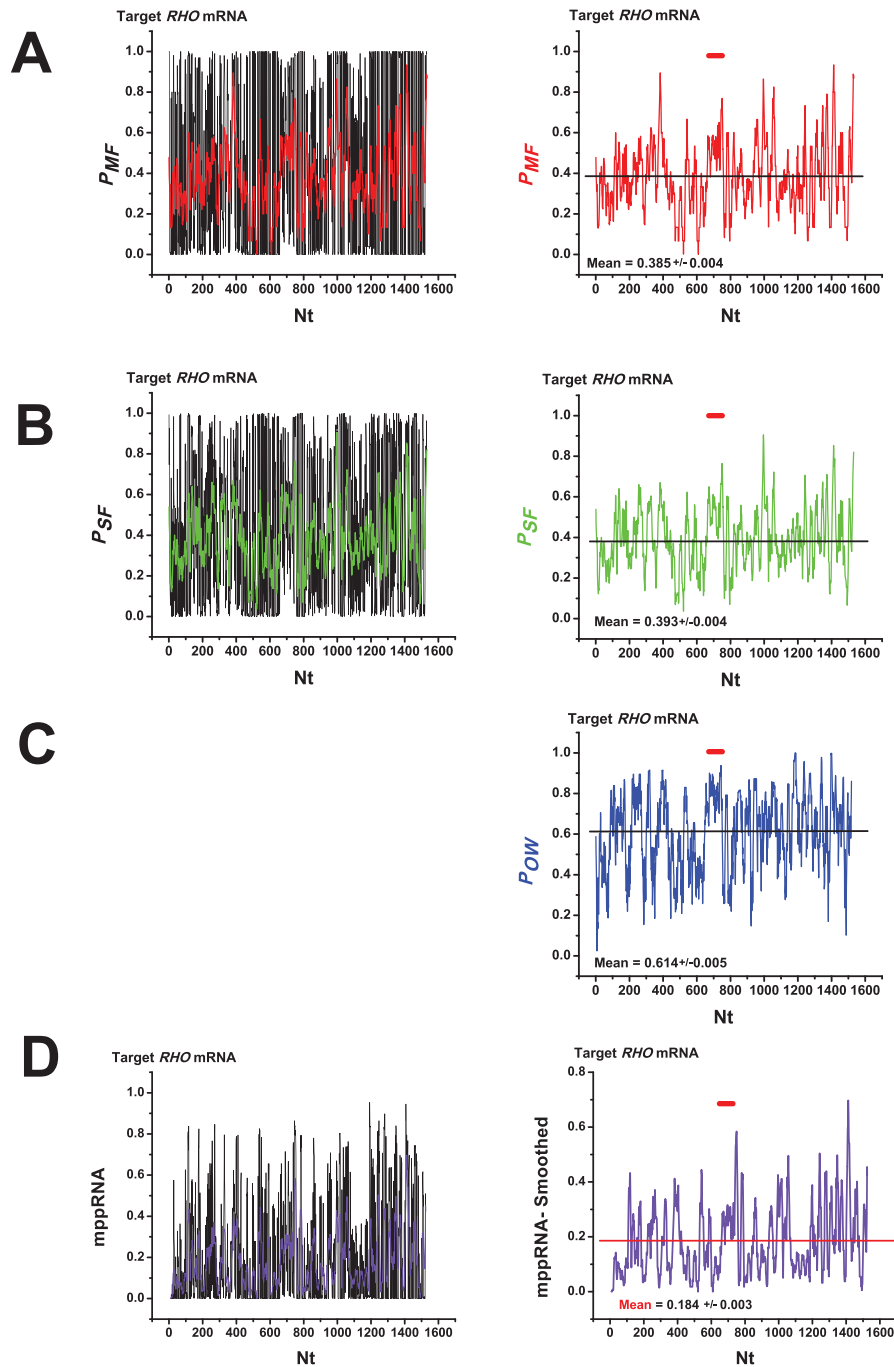


Figure 3. In silico prediction of target hRHO mRNA accessibility. (A) *Left panel* shows map of accessibility by Mfold mapping (*black trace*) and with 15-nt nearest neighbor averaging (*red trace*). *Right panel* shows Mfold average probability of access across hRHO mRNA. (B) *Left panel* shows map of accessibility by SFold mapping (*black trace*) and with 15 nt averaging (*green trace*). *Right panel* shows SFold average probability of access across hRHO mRNA. (C) *Right panel* shows 15-nt average OW probability across hRHO mRNA (*blue trace*). (D) *Left panel* shows map of accessibility by mppRNA mapping (*black trace*) and with 15 nt averaging (*violet trace*). *Right panel* shows mppRNA average probability of access across hRHO mRNA. In the averaged (*right side*) panels the weighted region of the site of maximum probability access eventually proven (653–763) is shown by a *red bar* in the upper aspects of the panel. The averaged values across the Mfold, SFold, OW, and mppRNA maps (*right panels*) are shown as a line.

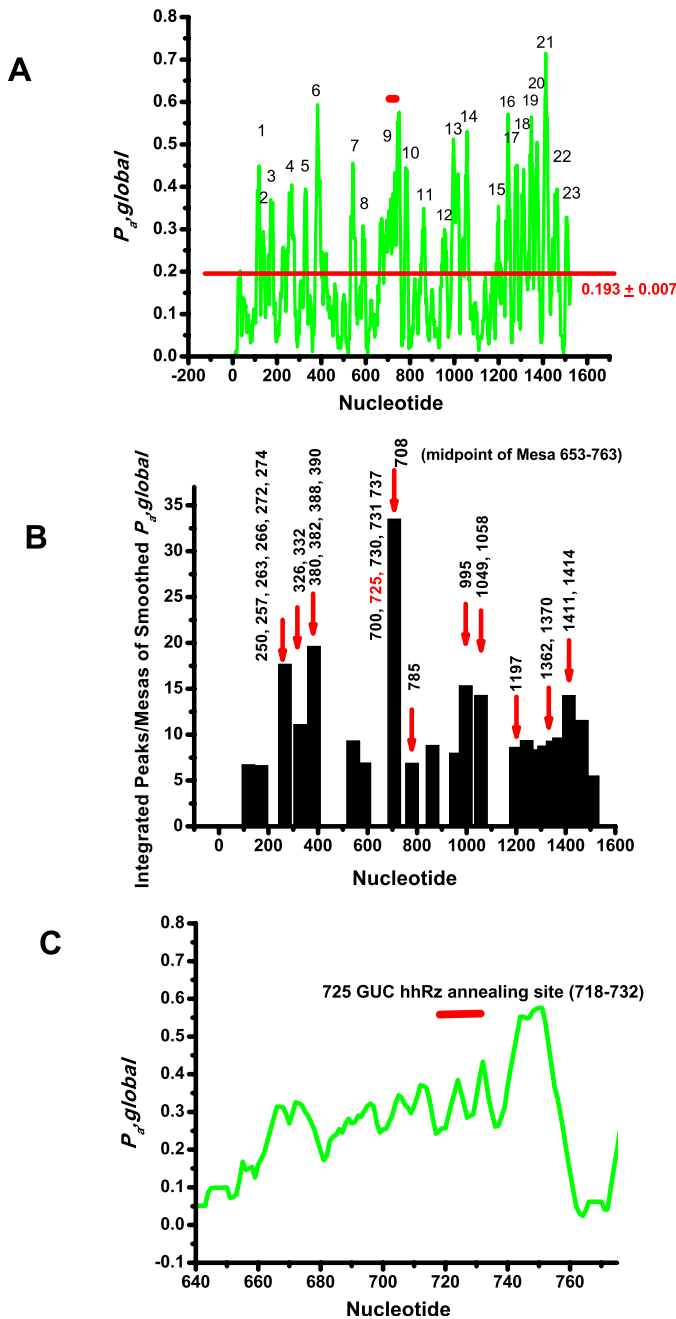


Figure 4. MppRNA analysis of accessibility. (A) The 15-nt average mppRNA map (Fig. 3D above) is expanded to show the mean of the map (red bar) and 23 accessibility peaks of the map that rise above the mean value. The horizontal red bar is the targeting region of the 725-hhRz lead candidate in this study. (B) Shows the integrals of the peaks from (A) and the different hhRz NUH \downarrow cleavage sites (numbers) located within the regions of each peak. Note that the “708” peak has the largest weight of all regions in the hRHO mppRNA map and represents a broad region of high accessibility; the 725 cleavage motif resides within this region, which covers approximately 110 nt. (C) Shows the expanded region of accessibility (653–763 nt) in detail and the location (red bar) of the annealing site for the 725 hhRz with 7-nt antisense flanks on each side of the cleavage nt.

Predicted accessible sites were tested for experimental accessibility in vitro using both the gsMAST and cMARS methods. gsMAST antisense tag target sites (Table 2) were chosen from predicted accessible regions along with a control tag containing mismatches to the *RHO* 565 target site. Correspondence of the gsMAST tags with regions of accessibility predicted for the *hRHO* mRNA by SFold are shown (Supplementary Fig. S2A). The structure of a gsMAST tag and its use are also shown schematically (Supplementary Fig. S2B). After competitive hybridization and washing of target bound on beads, the temperature-eluted tags were PCR amplified (Taq polymerase), with primers complementary to the constant 5' and 3' regions of each gsMAST antisense tag (double stranded regions), TA-cloned into linearized plasmid, transformed into competent bacteria, and clonal plasmid DNA samples were sequenced. Nine regions were found to be accessible by gsMAST (region 250, 310, 380, 725, 820, 995, 1050, 1190, and 1365; Table 2). Independently, the cMARS approach strongly confirmed regions around 250, 310, 380, 725 (data not shown). While there is solid correlation among computational and experimental approaches of target mRNA accessibility, a 10th target region (region 1411 in the 3'UTR) was not identified with gsMAST or cMARS methods, but had high computationally predicted accessibility and was successfully targeted by hhRz in a previous study by this lab.¹⁶ The reasons for this disparity are not understood. All 10 regions were subjected to hhRz agent screening in order to identify the best lead-candidate site for *hRHO* RNA drug development.

Efficient Screening of Large Libraries of Ribozymes for Lead-Candidate Identification

We identified potential hhRz NUH \downarrow cleavage sites within regions of predicted and experimental accessibility, and additional control regions with predicted and experimental low accessibility. We then designed a large series of hhRzs using the evolutionarily conserved enzyme core, adding a stabilized stem II (6 bp) to help facilitate hhRz folding,¹⁶ and adding 5' and 3' antisense flanks for molecular recognition of the target mRNA. In the initial screen we did not add any supportive upstream tertiary accessory elements (TAE). We ligated hhRz sequences within the engineered central domain of the VAI RNA scaffold. The targeting sequences within full-length *hRHO* are presented (Table 1). The initial goal was to experimentally identify the lead agent that promoted the

Table 2. gsMAST Tags Targeting *hRHO*

Region Name	<i>RHO</i> Target Region	<i>RHO</i> mRNA Target Sequence
250	258–275	5'-AACU <u>UCCUCACGCUCUAC</u> -3'
250	249–266	5'-U <u>UCCCCA</u> UCAACU <u>UCCUC</u> -3'
250	264–281	5'-CUCACGCUCUACGCACC-3'
310	309–326	5'-CUCAACUACA <u>UCCUGCUC</u> -3'
310	314–331	5'-CUACA <u>UCCUGCUCAACCU</u> -3'
356	348–365	5'-UUCAUGGUCCUAGGUGGC-3'
380	375–392	5'-ACCCUCUACACCUCUCUG-3'
565 (mismatch)	566–583	5'-TGCCT <u>C</u> CACCTGAGTCAT-3'
660	671–668	5'-UCGACUACUACACGCUCA-3'
660	695–712	5'-CGAGUCUUUUGUCAUCUA-3'
660	666–683	5'-UACUACACGCUCAAGCCG-3'
660	689–706	5'-CAACAACGAGUCUUUUGU-3'
725	725–739	5'-CCACUUCACCAUCCCGAU-3'
740	737–754	5'-CCCGAUGAUUAUCAUCUU-3'
785	775–792	5'-UCUCACCGUCAAGGAGG-3'
820	813–830	5'-UCAGCCACCACACAGAAG-3'
995	987–1004	5'-GCCGCCAUCUACAACCCU-3'
1050	1050–1067	5'-ACCACCAUCUGCUGCGGC-3'
1190	1189–1206	5'-UACACCUUCCCCAGCCA-3'
1340	1339–1356	5'-ACCAAGACCUACUGAUCU-3'
1360	1365–1382	5'-ACGUUCCCCAAGGCCAGC-3'
1411	1403–1420	5'-UCCCAACUCAUCUUUCAG-3'

Sense sequences of 18-nt regions within *hRHO* to which gsMAST tags (antisense) were designed are shown. Targeted sequences of eluted antisense gsMAST tags, which are in experimentally accessible regions, were recovered by TA-cloning and sequencing, and are shown in bold. The 785 and mismatched 565 probes were negative control target sequences, with the 785 site predicted to be inaccessible, and the mismatched 565 sequence (mismatched bases are underlined) unable to anneal under physiologic conditions. Control antisense tags were never found in sequencing of PCR-amplified, eluted gsMAST tags.

greatest target knockdown capacity in human cells. Thirty-three hhRz NUH↓ cleavage sites within 10 regions were screened for sensitivity to hhRz cleavage using a cell-based screening platform, established in this lab, which exploits the SEAP reporter.¹⁷ A bicistronic vector (p*RHO*-IRES-SEAP) was designed using an IRES sequence to produce a single (bicistronic) mRNA transcript able to express both *hRHO* and SEAP proteins (Fig. 2). The full-length *hRHO* cDNA (transcription start to immediately upstream of the first dominant polyA signal) was placed upstream of the IRES sequence with the SEAP cDNA downstream. RNA secondary structure begins to emerge during transcription (co-transcriptional), so placing the target mRNA upstream of the reporter is expected to favor folding of the target mRNA into native states independent of both the downstream IRES (insulator) and the reporter SEAP components.¹⁷ The stable SEAP reporter protein is secreted

into culture medium in proportion to its cellular steady-state mRNA levels making it an ideal “model” target mRNA for assaying impact of PTGS agents on gene expression over time in live cell cultures.³⁹

The hhRz design used a symmetrical 7-nt antisense flanks surrounding the catalytic consensus core and with the secondary folded structure stabilized by an extended (6 bp) stem II helix capped by an ultrastable UUCG loop (RzA6 design, hhRz schematic Supplementary Fig. S3A).^{16,17} HhRz cDNAs were efficiently cloned into the pNEB-VAI-hhRz-1 (pUC-VAL) expression vector with an established high-efficiency, positive-selection approach (see Supplementary Methods).¹⁷ The modified VAI scaffold RNA allows high expression and trafficking of the embedded ribozyme into the cytoplasm due to the very strong intragenic A/B box RNA Pol-III promoter of the VAI RNA and the trafficking element of the basal stem. The pNEB-VAI-hhRz-1 expression plasmids were

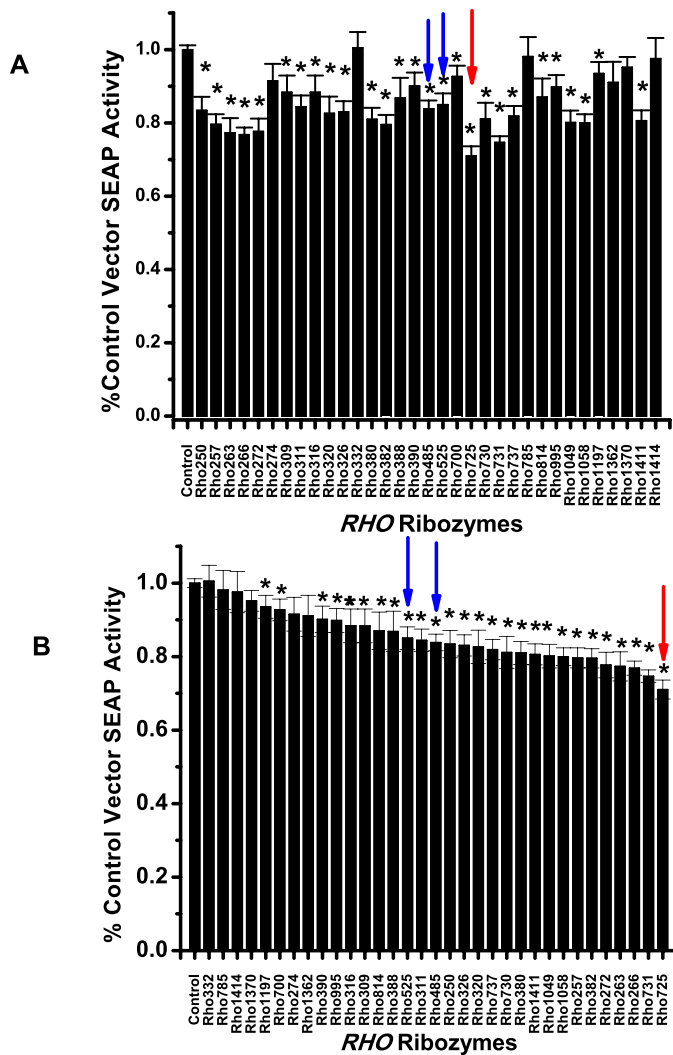


Figure 5. *RHO* hhRz *RHO*-IRES-SEAP screen. (A) HEK293S-*RHO*-IRES-SEAP cells were transiently transfected with VAI-hhRz-1 (pUC-VAL) constructs expressing hhRzs targeting NUH sites in the 10 chosen predicted accessible regions. Half (75 μ L) of the culture media was removed and replaced 24 hours posttransfection. SEAP protein levels were assayed using the SEAP reporter assay on conditioned culture media removed 72 hours posttransfection. Mean percent control VAI (without hhRz) vector transfection SEAP activity is shown \pm SEM (one-way ANOVA $F = 7.55$, $P < 0.001$). Asterisks indicate significant ($P < 0.05$) knockdown relative to control transfection by individual parametric t -tests (Fisher). The red arrow shows the knockdown by the 725 hhRz construct while the blue arrows show the knockdown by the related 485 and 525 hhRzs from a prior study⁶ (these target the same site but differ in antisense flank lengths). (B) Rank ordering of knockdown by the set of hhRzs in the screen. Asterisks and arrows indicate as in (A). The 725-GUC targeting hhRz is the lead knockdown agent in the screen.

transiently transfected into stable HEK293S-*RHO*-IRES-SEAP cells in 96-well plates. Media was removed at 24 hours posttransfection and replaced with fresh media in order to improve sensitivity and dynamic range of the assay (by removing some of the SEAP protein that is made before expression of VAI-hhRzs). SEAP enzyme activity was assayed 72 hours posttransfection with a fluorescent SEAP enzyme assay. This approach has been shown to have a low coefficient of variation (relative to Western analysis) to efficiently evaluate ensembles of hhRz or shRNA agents to identify a lead candidate.¹⁷

Thirty-three hhRz NUH \downarrow cleavage sites in *hRHO* (Table 1) were screened for sensitivity to hhRz suppression using the cell-based screening platform with the p*RHO*-IRES-SEAP vector stably transfected into HEK293S cells. These agents targeted NUH \downarrow motifs in the coding region and the 3' untranslated region of full-length *hRHO* mRNA. SEAP suppression was measured relative to the control construct of the VAI scaffold without an embedded hhRz sequence (expression normalized to 1.0) and is shown for all constructs in their sequential order of appearance along the *RHO* target (Fig. 5A). Mean percent control of VAI (without hhRz) transfection SEAP activity is shown \pm SEM. The one-way ANOVA refuted the null hypothesis that all of the constructs exerted the same knockdown of target ($F = 7.55$, $P < 0.001$). Variance was found to be uniform throughout all samples by two of three statistical tests (Levene absolute variation test, $F = 1.6520$, $P = 0.0132$; Levene square deviation test, $F = 1.0633$, $P = 0.3741$; Brown Forsythe, $F = 1.1242$, $P = 0.2920$), and data for each construct and control were found to be normally distributed (Gaussian) by Kolmogorov-Smirnov test. Therefore, post hoc parametric t -tests were used to compare each hhRz construct relative to control, from many independent analyses (see Table 3). Post hoc parametric t -tests (single-step Bonferroni, Tukey, Fisher, Holm-Bonferroni; the latter is a more powerful modification than the Bonferroni correction for multiple comparisons that addresses the family wise Type I error rate) evaluated whether individual constructs showed knockdown relative to control transfection with pNEB-VAI-1 (pUC-VAL without hhRz; criterion significance preset at $P < 0.05$). Of the 33 hhRz constructs screened by cellular transfection into HEK293S-*RHO*-SEAP cells relative to control (pNEB-VAI-1 or pUC-VAL), 16 (48.4%) showed significant reduction (knockdown) of SEAP protein expression by Bonferroni and Holm-Bonferroni analysis, 17 (51.5%) showed significant knockdown

Table 3. Statistical Evaluation of hRHO-IRES-SEAP Screen of hRHO hhRzs

Construct	SEAP Knock-Down	SD	SEM	<i>P</i> Value, Bonferroni	<i>P</i> Value, Tukey	<i>P</i> Value, Fisher	<i>P</i> Value, Holm-Bonferroni	<i>N</i>
pUCVaL	1	0.14066	0.01202	—	—	—	—	137
Rho250	0.83416	0.17872	0.03727	3.61961E-4	3.32177E-4	6.45207E-7	6.45207E-7	23
Rho257	0.79633	0.13437	0.02743	3.33977E-7	3.32596E-7	5.95325E-10	5.95325E-10	24
Rho263	0.77336	0.15792	0.03948	4.14028E-6	4.05762E-6	7.38018E-9	7.38018E-9	24
<i>Rho266</i>	0.76834	0.10369	0.01925	2.12291E-11	1.28452E-8	3.78415E-14	3.78415E-14	29
Rho272	0.777	0.13864	0.03466	7.06944E-6	6.89221E-6	1.26015E-8	1.26015E-8	16
Rho274	0.91531	0.1297	0.04585	1	1	0.11223		8
Rho309	0.88347	0.1846	0.04615	1	0.4333	0.00269		16
Rho311	0.84439	0.12171	0.03043	0.03603	0.02512	6.42157E-5	6.42157E-5	16
Rho316	0.88357	0.22501	0.04593	0.19657	0.10527	3.50393E-4		24
Rho320	0.82641	0.18099	0.04525	0.00478	0.00395	8.51337E-6	8.51337E-6	16
Rho326	0.83036	0.14101	0.02878	1.24271E-4	1.16833E-4	2.21517E-7	2.21517E-7	24
Rho332	1.00498	0.17291	0.04323	1	1	0.89754		16
Rho380	0.80977	0.08255	0.0312	0.47428	0.20511	8.45416E-4		7
Rho382	0.79538	0.12344	0.02632	1.1158E-6	1.10673E-6	1.98895E-9	1.98895E-9	22
Rho388	0.86838	0.15535	0.05492	1	0.84704	0.0137		8
Rho390	0.90153	0.14402	0.03601	1	0.80178	0.01114		16
Rho700	0.92696	0.14468	0.02953	1	0.94134	0.02449		24
<i>Rho725*</i>	0.71025	0.12092	0.02578	2.92868E-14	1.73841E-8	5.22046E-17	5.2205E-17	22
Rho730	0.81138	0.19898	0.04342	3.10549E-5	2.98318E-5	5.53563E-8	5.53563E-8	21
<i>Rho731</i>	0.74663	0.08065	0.01719	9.22925E-11	1.24369E-8	1.64514E-13	1.64514E-13	22
Rho737	0.81902	0.10663	0.02753	0.00367	0.00308	6.54682E-6	6.54682E-6	15
Rho814	0.87031	0.19638	0.05071	0.66454	0.25956	0.00118		15
Rho995	0.898	0.12584	0.03249	1	0.79125	0.01064		15
Rho1049	0.80136	0.08525	0.03222	0.27758	0.13782	4.94802E-4		7
Rho1058	0.7998	0.09194	0.02374	3.60065E-4	3.30483E-4	6.41827E-7	6.41827E-7	15
Rho1197	0.93525	0.12487	0.03122	1	1	6.41827E-7		16
Rho1362	0.91085	0.15819	0.05593	1	1	0.09458		8
Rho1370	0.95176	0.08012	0.02833	1	1	0.3653		8
Rho1411	0.806	0.13741	0.02865	3.67124E-6	3.60153E-6	6.54409E-9	6.54409E-9	23
Rho1414	0.97563	0.22482	0.0562	1	1	0.52881		16
Rho785	0.98133	0.15	0.05303	1	1	0.72608		8
Rho485	0.83849	0.08984	0.02246	0.01895	0.01412	3.37831E-5	3.37831E-5	16
Rz525	0.8503	0.12188	0.03047	0.06719	0.04327	1.19774E-4		16

The name of the construct, the level of expression of the SEAP reporter, the SD and the SEM is shown for each construct. Bonferroni, Tukey, Fisher, and Holm-Bonferroni *P* values are shown for each construct (there are no cell entries (—) for pUCVal because this is the negative control construct). As the Holm-Bonferroni test is a multiple comparison test only the significant *P* values are shown (cells with non-significant *P* values are left blank). The number of replicates for each construct is shown in the last column. The hhRzs that promote statistically significant knockdown relative to control by at least one statistical test are bold in the first column. The three top leads (725 GUC↓, 731 UUC↓, 266 CUC↓) are in bold-italic with the lead candidate indicated by an asterisk.

by Tukey analysis, and 26 (78.8%) showed significant knockdown by Fisher analysis (Table 3, Fig. 5A). Further (internal) validations occurred with the finding of no significant knockdown (by all 4 post

hoc *t*-tests) by a hhRz targeting GUC↓ 785 used previously and known not to cause cellular *hRHO* suppression, and no significant knockdown (by all 4 post hoc *t*-tests) by a hhRz targeting CUA↓ 332,

which is located in a structured stem region of low accessibility that did not previously support adjacent hhRz-mediated target knockdown (hhRz GUC↓ 356, see fig. 6 of Ref. 16).

The level of SEAP protein activity suppression was then rank-ordered from lowest to highest levels of suppression (Fig. 5B). A lead candidate hhRz targeting the GUC↓ motif at 725 in full-length human *RHO* showed a 28.97% knockdown of SEAP reporter protein activity in the stable HEK293S-*RHO*-IRES-SEAP cell line at the 72-hour time point (red arrow). We estimate that the maximum suppression achievable in this strategy is only approximately 50% suppression due to use of a stable expressing cell line with preformed levels of target bicistronic mRNA and protein in processing, translation, and secretion streams.¹⁷ The novel 725 target site has never been targeted by any therapeutic PTGS agent and there are no known *hRHO* mutations at this site, making it an ideal candidate site for MI PTGS therapy.²⁸ The hhRz targeting the nearby UUC↓ motif at 731 is also a strong suppression agent. Significant suppression is also achieved at other NUH↓ sites in this neighborhood (CUU↓ 730, AUC↓ 737). This is consistent with the expected broad region of accessibility in the human *RHO* mRNA around the 725 site as predicted by mppRNA (653–763; see Fig. 4C). The hhRz targeting the CUC↓ motif at 266 is also a strong agent (third most potent of those tested). A hhRz targeting 266 was shown to be effective at human *RHO* protein suppression in our prior study when also expressed within a modified VAI scaffold RNA (pgVAL VAI RNA scaffold).^{10,16} Similarly, the hhRz targeting 1411 was effective in the prior study and is tenth in rank order in this study.

Two of the hhRz agents (GUC↓ 485, GUC↓ 525; blue arrows) were tested in a prior study for an allele-independent (MI) therapy for *RHO* mutations and showed efficacy to transiently reduce the rate of retinal degeneration in a rat model expressing a mutant mouse P23H *RHO* mRNA and protein.⁶ These hhRzs were expressed without a scaffold from an *RHO* promoter (RNA Pol-II transcribed) in this prior study. We note that the hhRz 525 in our study (with VAI scaffolding) is the exact form of the antisense flanks used in the prior study⁶ (5-nt 5' flank/6-nt 3' flank), whereas the hhRz 485 targets the same GUC↓ site but has balanced 7-nt/7-nt antisense flanks as used for all other hhRzs tested in this study. The 525 site in the mouse and dog *RHO* mRNAs is equivalent to site 485 in *hRHO* mRNA. Both hhRzs in this study target the same GUC↓ motif at 485 in

human *RHO* mRNA. Expressed within the VAI scaffold RNA, the lead agent at 725 shows greater suppression potential in the *hRHO*-IRES-SEAP assay than the 485/525 hhRzs against full-length human *RHO* mRNA as a component of the bicistronic mRNA used in the screen (725 vs. 485 hhRz: $t = -3.58$, $P = 0.001$; 725 vs. 525 hhRz: $t = -3.51$, $P = 0.001$).

We examined the correlation between the extent of knockdown by the HTS assay and the predicted accessibility (Fig. 6A). The level of suppression at the particular site is plotted versus the weight of the integral for the peak that contains the NUH↓ cleavage site (Fig. 4B). There is solid and significant correlation between the predicted accessibility of the peak regions and the level of target suppression at specific NUH↓ sites within each region. The line fitted to the data through the origin ($x = 0$, $y = 0$; control has no knockdown and no meaningful accessibility) has non-zero slope (0.808 ± 0.027 SEM) and with a strong adjusted R^2 (0.84859) with statistical significance (ANOVA, $F = 169.1$, $P = 1.252 \times 10^{-13}$). We also compared the integrated area under the curve for each hhRz annealing site (15-nt span) relative to the percentage target knockdown obtained for each hhRz (Fig. 6B). The line fitted to the data through the origin (control has no knockdown and no meaningful accessibility) has non-zero slope (0.17916 ± 0.02192 SEM) and with a solid adjusted R^2 (0.666) with statistical significance (ANOVA, $F = 66.78$, $P = 2.47 \times 10^{-9}$). These findings indicate that the mppRNA approach to predicting accessibility is a reliable means to begin the process of screening for lead PTGS agents. We note, however, the variation in cell-based knockdown at NUH↓ sites within single regions of accessibility predicted by peak integration. For example, several hhRzs targeting within the “250” region were tested and these show varying levels of suppression and statistical significance. This region is expected to contain a large, single-stranded loop capping a stable stem secondary structure (Fig. 6C, adapted from Ref. 16). The variation in activity at different local NUH↓ sites in a single accessible region may reflect the varying propensity of different NUH↓ motifs to support cleavage,^{41–43} or variation in accessibility within a single large region, which could occur due to impact of boundary stable regions on regions of secondary structural accessibility, or variation in tertiary structure within these regions may constrain uniform access to binding. Using 3D RNA modeling (RNA composer) of the region we find a significant tertiary structure in which the

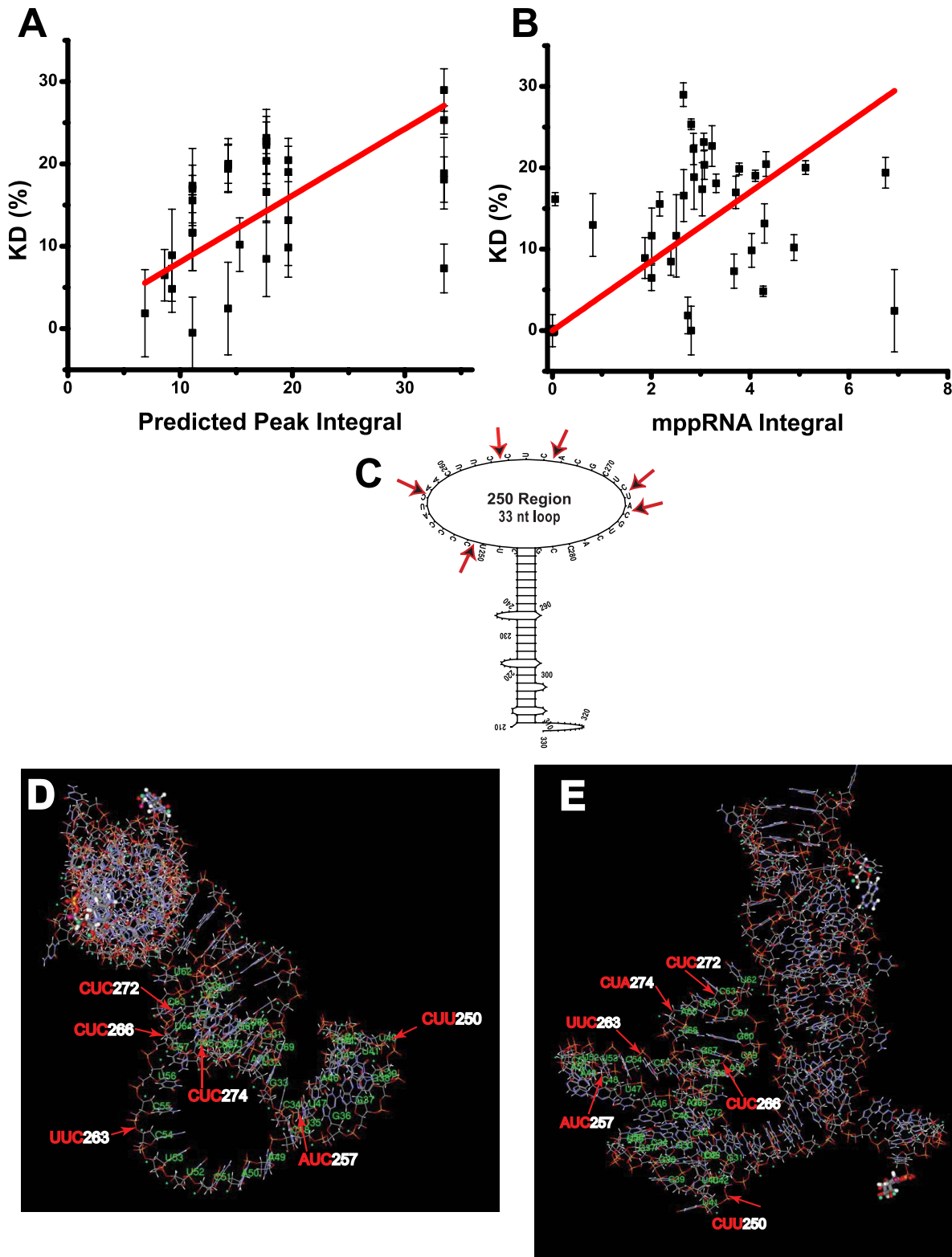


Figure 6. Experimental knockdown is proportional to predicted accessibility. (A) The percent knockdown of SEAP in the screen is assessed relative to the weight of the integral of the peak in the mppRNA map that contains a given hhRz NUH \downarrow site. The *line* fitted to the data through the origin (control has no knockdown and no meaningful accessibility) has nonzero slope (0.808 ± 0.027 SEM) and with a strong adjusted R^2 (0.84859) with statistical significance (ANOVA, $F = 169.1$, $P = 1.252 \times 10^{-13}$). (B) The percent knockdown of SEAP is assessed

← relative to the weight of the integral (area under curve of the mppRNA map) for the specific annealing site of a given hhRz. The *line* fitted to the data through the origin (control has no knockdown and no meaningful accessibility) has nonzero slope (0.17916 ± 0.023 SEM) and with a solid adjusted R^2 (0.666) with statistical significance (ANOVA, $F = 66.78$, $P = 2.47^{E-9}$). (C) Shows a predicted 2D folding (MFold) of the 250 region of hRHO that contains multiple NUH↓ cleavage sites, some of which were targeted in this study (*arrows*). (D, E) Shows a 3D predicted folding (RNA Composer) from two approximately orthogonal perspectives of the 250 region. This region (peak 4 in Fig. 4A) has the largest variability in the relationship between KD at a particular NUH↓ motif and the single predicted peak weight. The identity of the nucleotides is shown in the labels and the location of the individual NUH↓ cleavage sites in the region are shown. The expected basal helix is seen end-on in (D) and from the side (E). Accessibility in the predicted 2D loop demonstrates complexity at the predicted 3D level. It is the 3D complexity that is likely more relevant to PTGS annealing.

accessibility to annealing to cleave at different sites could have substantial variation (Figs. 6D, 6E).

Having identified our lead 725 agent in a fusion RNA using reporter elements, we tested for in vitro and in cellula functionality of the lead construct against *hRHO* mRNA without reporter elements. We investigated, qualitatively, the extent to which the 725 hhRz within VAI scaffold RNA was able to cleave *hRHO* target mRNA through in vitro co-transcription/cleavage assays where the VAI-hhRz and the target RNAs are transcribed simultaneously from linearized plasmids.² Both the hhRz (within the VAI scaffold) and the *hRHO* target element RNAs are transcribed with T7 RNA polymerase from a T7 promoter immediately upstream of the encoding sequences within the plasmids. The *hRHO* target element is transcribed from a fraction (450-bp PstI/StuI fragment) of the full-length human *RHO* cDNA ligated into pBlueScript plasmid; T7-mediated transcription with additional boundary vector sequences results in a 511-nt target RNA. The location of the 725 GUC↓ cleavage site is asymmetrically located in this target *RHO* RNA element, which allows identification of two cleavage products of differing size on denaturing RNA gels (371 and 140 nt). In silico RNA folding assays (mppRNA) indicated that the region around the 725 cleavage site shows similar but not identical accessibility in the short *RHO* target when compared with the full-length native dominant mRNA (Supplementary Fig. S4). The 725 hhRz with the stabilized 6-bp stem II region is able to cleave the target mRNA, at the expected position of the 725 GUC↓ motif, which leads to two products of expected size (Fig. 7A; $n = 2$). Catalytic core mutation of this hhRz (*G12C*) completely obviated cleavage as expected. In vitro, a substantial fraction (~40%) of the target element is cleaved but not to completion under conditions when the 725 VAI scaffold-hhRz is in substantial excess. The etiology of the incomplete cleavage in vitro under conditions of enzyme excess is not yet clear. However, using short-substrate or full-

length *hRHO* mRNA transcribed in vitro run on nondenaturing gels we find more than a single RNA conformational band for both the short- and full-length *hRHO* targets (Fig. 7B). This suggests that the two *hRHO* substrates can enter into more than a single conformation. Whether the accessibility of the target regions varies in discrete conformational states remains to be determined for both in vitro and in cellula cases. Fractions of the target with inaccessible regions, for example due to overarching tertiary folding, could cap the maximum cleavage fraction in vitro because other potentially relaxing forces (e.g., heterogeneous RNA protein binding) are not present.

We tested for the capacity of the VAI-hhRz-725 to suppress full-length *hRHO* mRNA in cellula. A cellular cDNA expression construct was generated that contained the full sequence of the dominant mRNA transcript of *hRHO*, with full 5' and 3'UTR regions up to and just distal to the dominant poly A site, and under the control of a strong CMV promoter (in pCDNA3.1), which was engineered to initiate Pol-II transcription at the target mRNA start site. Transient co-transfections of VAI-hhRz chimeras and full-length *hRHO* target were performed in HEK293S cells, and *hRHO* mRNA levels were assessed by an established quantitative real-time reverse transcription-PCR assay (qRT-PCR) standardized by a set of *hRHO* plasmids in varying amounts.^{16,17} The stem II stabilized hhRz targeting *RHO* 725 (R725RzA6) in pUC-VAL (VAI-hhRz-1) suppressed full-length *RHO* mRNA target in HEK293S cells (26.1% knockdown of *RHO* mRNA levels compared with control vector transfection, *t*-test, $P = 0.053$; replicates: pUC-VAL, $n = 3$; R725RzA6, $n = 6$; inactive R725RzA6In, $n = 6$; Fig. 7C). This level of suppression is proportional to that seen for the same hhRz-VAI expression construct used in the *hRHO*-IRES-SEAP screen (~29%). A catalytic inactive mutant (*G12C* mutation) for R725RzA6 showed knockdown (18.1%) of *RHO* mRNA in cells that was not significantly different from control (*t*-test, $P = 0.193$). There was an 8% difference in suppression

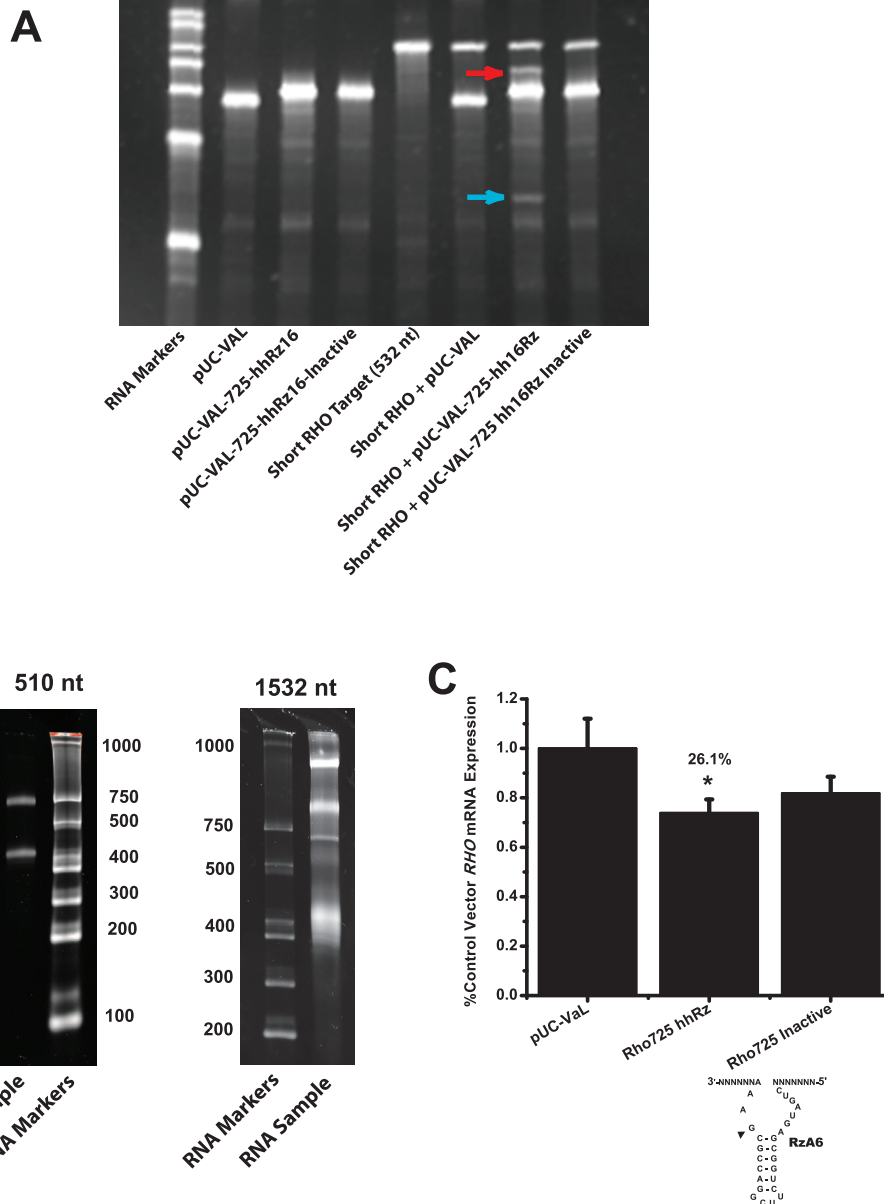


Figure 7. In vitro and in cellula 725 ribozyme cleavage assays-stem-II optimization. (A) In vitro transcription/cleavage reactions were performed and run on a 5% denaturing PAGE gel with 8 M urea relative to RNA size markers (lane 1). The mobility of the scaffold and active and inactive (G12C) ribozymes (lanes 2–4) and the short RHO substrate (511 nt; lane 5) are shown. Cleavage products of 371 nt (*red arrow*) and 140 nt (*blue arrow*) are only identified with a catalytically active 725 hhRz 16 is embedded in the scaffold (lane 7) but not from the pUC-VAL scaffold itself (lane 6) or with a 725 hhRz 16 that had a catalytic core inactivating mutation (G12C; lane 8). (B) In vitro analysis of short *hrHO* (511 nt) and full-length (1532 nt) *hrHO* mRNAs, transcribed in vitro but analyzed on nondenaturing PAGE gels relative to RNA size mobility markers. For the short *hrHO* (*left panel*) there are two prominent bands. For the full-length *hrHO* (*right panel*) there appear to be at least three well-populated conformational states. (C) In cellula assay to assess target *hrHO* mRNA knockdown in the pUC-VAL scaffold. HEK293S cells were transiently co-transfected with pNEB-VAL-hhRz-1 and pRHO-fix5UT. Total RNA was extracted from transfected cells 48 hours posttransfection and analyzed for relative *hrHO* mRNA levels using qRT-PCR. Mean percent control vector transfected cells *hrHO* mRNA levels are shown \pm SEM (one-way ANOVA $P = 3.54$, $P = 0.03$). Asterisks denote significant ($P < 0.1$) knockdown relative to control. The R725RzA6 directed at the lead candidate site showed moderate knockdown of *hrHO* mRNA (26.13% knockdown, $P = 0.053$, $n = 6$). Similar to results seen in hhRz targeting SEAP,¹⁷ the catalytically inactive mutant (G12C) of R725RzA6 did not strongly reverse this knockdown effect ($P = 0.38$ active versus inactive R725RzA6, $n = 6$), suggesting the knockdown was likely due to an antisense or catalytic antisense effect. A 4-bp stem-II hhRz (R725RzA4), with stem-II loop from a well-studied hhRz (HH16)^{45,46} showed an improvement in RNA knockdown (49.40% knockdown, $P = 0.033$, $n = 3$), which was reversed by the G5C mutation ($P = 0.45$ versus control, $n = 3$).

between the catalytically active 725RzA6 and the inactive hhRz in the pUC-VAL scaffold but this was not significant (t -test, $P=0.378$). The lack of difference in suppression between the active and inactive hhRzs could be related to the extent of knockdown achieved, or an inhibitory effect on catalysis due to structural stabilization of the hhRz with the 6-bp extended stem-II,⁴⁴ and a residual antisense effect in cellula with hhRz catalytic core mutation.

Rational Lead Hammerhead 725 Ribozyme Optimization

The VAI expression construct (VAI-hhRz-1, pUC-VAL) used in the screen was designed to provide a large (49 nt) single-stranded harbor for hhRz expression within a disrupted central domain of the otherwise structured and stable VAI RNA scaffold (Fig 1B). The VAI scaffold, also with a disrupted central domain, had been used successfully in prior studies in this and other labs.^{10,16} However, several simpler VAI scaffold designs were established for hhRz expression and support.³⁵ Therefore, we worked to evaluate whether a different VAI chimera design beyond pUC-VAL would improve the efficacy of our lead 725 hhRz candidate. We chose the VAI Prislei- δ design in which the entire central domain was effectively deleted to maintain only a short asymmetrical bulge loop between the apical and basal stems. Also, the 6-bp stabilized stem II hhRz may have an inhibitory effect on catalysis in cellula (e.g., by perturbing essential core hhRz conformational changes) as suggested above and in prior studies.^{16,17,44} Therefore, we evaluated the extent to which a 725 hhRz with a simpler classical 4-bp stem II and loop design (725RzA4), modeled after the same components in a prior construct (HH16),^{45,46} would enhance catalysis. We first compared the 4-bp stem II 725 hhRz, with 7-nt antisense flanks on both sides of the cleavage nt, and embedded in the VAI-hhRz-1 (pUC-VAL) and VAI-hhRz-2 (pPrislei) scaffolds in in vitro cleavage assays. We found that the 725 HH16 hhRz exerted greater cleavage of target (~ 2 -fold) at the expected site in vitro when embedded in the VAI-hhRz-2 (Prislei- δ VAI) scaffold (Fig. 8A). Again, as expected catalytic core mutation (*G12C*) obviated cleavage. We tested the 4-bp stem II 725 hhRz (design in Supplementary Fig. S3B) for its capacity to suppress *hRHO* mRNA when expressed in the VAI-hhRz-1 and VAI-hhRz-2 scaffolds. In the VAI-hhRz-1 scaffold (pUC-VAL) the 4-bp Stem II 725 hhRz showed significant knockdown (49.40%; compared

with stabilized R725RzA6, Fig. 7C) of full-length *hRHO* mRNA in HEK293S cells compared with its empty scaffold control ($P = 0.034$, $n = 3$; Fig. 8B). Catalytic inactive mutant (*RzA4* inactive, *G12C* mutation) reversed the knockdown (mean 14.2%) from the R725RzA4 active hhRz construct relative to control ($P = 0.193$, $n = 3$). Reversal of cellular knockdown due to catalytic core enzyme mutation indicates that the suppression occurred by way of a true RNA catalytic effect (binding plus cleavage), as opposed to a pure antisense effect (binding alone or binding with cleavage but without product release). This showed that conformational stabilization of stem II (in R725RzA6) appeared deleterious to hhRz catalysis, perhaps because it limits flexibility of the enzyme to achieve catalytically active state(s), yet still permits a binding/antisense effect. The near 50% full-length target *hRHO* mRNA suppression via RNA catalysis with the 4-bp stem II 725 hhRz indicated its significant potential for further optimization as a candidate therapeutic hhRz. Using the other VAI chimera (VAI-hhRz-2, pPrislei- δ), we saw some improvement in the efficacy of the 4-bp stem II 725 hhRz (R725RzA4.2) to approximately 65% suppression in cells relative to empty Prislei scaffold control when the full-length *hRHO* mRNA was measured by qRT/PCR with an *hRHO* cDNA standard ($P = 1.69 \times 10^{-4}$; replicates: pPrislei- δ , $n = 15$; RzA4, $n = 28$; Fig. 8B). Again, catalytic core mutation (*G12C*) reversed knockdown toward control levels (23.8% suppression, $P = 0.1536$, RzA4Inactive, $n = 12$), which indicates the contribution of an RNA catalytic (cleavage) mechanism in cellular target *RHO* mRNA suppression. There was significant difference in comparing knockdown between catalytically active and inactive 4-bp stem II 725 agents in the pPrislei- δ scaffold (44.5%, $P = 3.22 \times 10^{-4}$). Investigating the knockdown between the 4-bp stem II between the two VAI scaffolds shows a substantial difference, but which was not significant (19%, $P = 0.181$). Given the modestly improved knockdown and the smaller RNA scaffold (less complexity) the 725 hhRz (4-bp stem II) pPrislei- δ VAI construct was preferred over pUC-VAL. To further validate the effect, we repeated the experiment for mRNA knockdown with the 725 hhRz (HH16) in the VAI-hhRz-2 (pPrislei) scaffold by identical transfection conditions but with an alternative $2^{-\Delta\Delta C_t}$ method of mRNA quantitation relative to β -actin housekeeping mRNA and showed substantial and significant *hRHO* mRNA knockdown (Supplementary Fig. S5).

Ribozymes embedded in the VAI-hhRz-2 scaffold

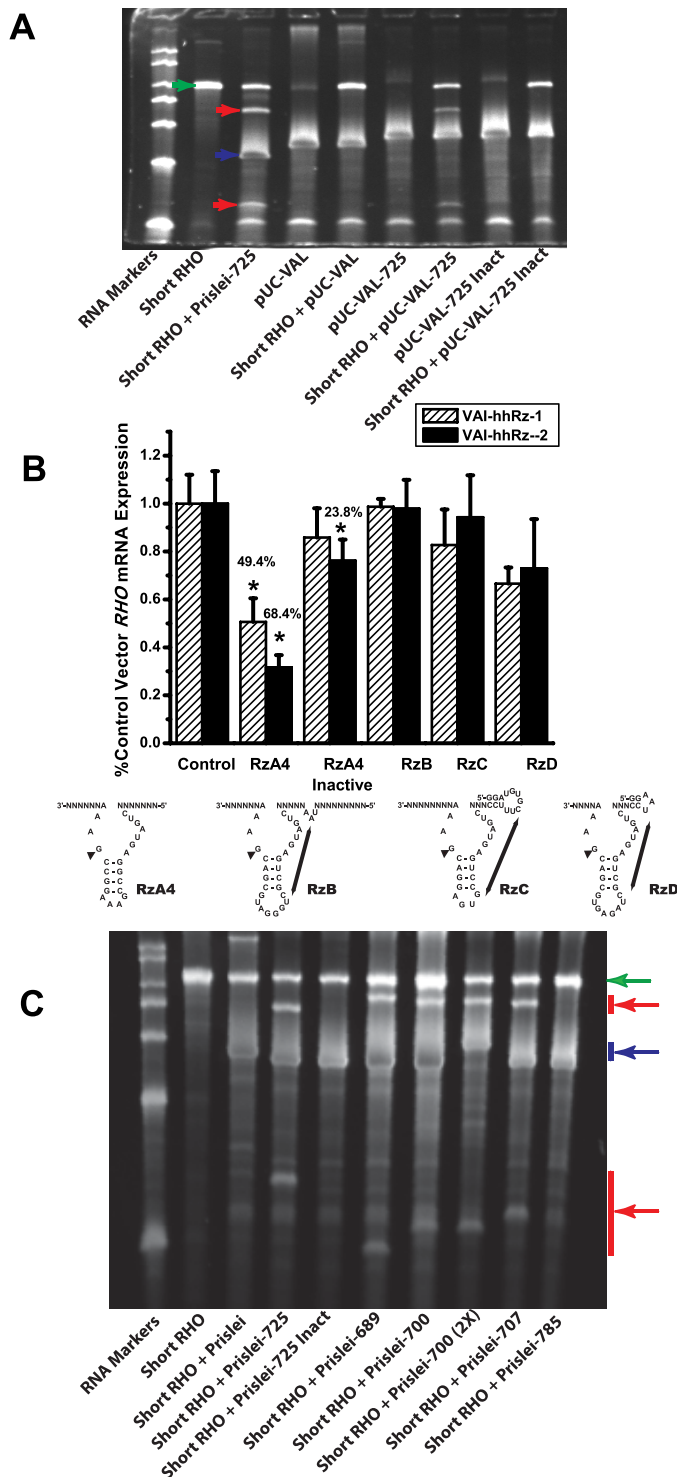


Figure 8. Rational optimization tests of the 725 hhRz. (A) In vitro co-synthesis with cleavage assay comparing the 725 hhRz with 4-bp stem II in the pPrislei versus pUC-VAL VAI RNA scaffolds against the short RHO target. Linearized plasmids in defined molar ratio (6:1 ribozyme:target) were transcribed by T7 RNA polymerase and cleavage emerged during the 3-hour incubation prior to analysis by PAGE-urea gel electrophoresis and staining with RNA dye (SYBR

that targeted other GUC↓ cleavage sites in the broad predicted 110-nt span accessible region around 725 (GUC↓ 689, GUC↓ 700, GUC↓ 707) were tested by in vitro cosynthesis/cleavage reactions where the ribozyme and substrate RNAs are transcribed simultaneously and react (Fig. 8C). All showed essentially equivalent cleavage as the GUC↓725 agent. Note that the 785 GUC↓ fails to cleave substrate *hrHO* RNA, which replicates results from our prior study for a hhRz targeting the same site in a prior VAI scaffold.¹⁶

Gold). Substrate short RHO is labeled (*green arrow*) and the mobility of the different scaffold-hhRz RNAs is labeled (*blue arrow*). Note that the extent of cleavage products (P1, P2) (*red arrows*) with the 725 hhRz within the Prislei VAI scaffold is greater than with the same 725 hhRz within the pUC-VAL VAI scaffold. There is no cleavage without the hhRz within the scaffold (not shown for pPrislei) and inactivating mutations in the catalytic core of the 725 hhRz (G12C) obviates cleavage (data not shown for pPrislei). Eight percent (wt/vol) PEG 8000 was used to simulate the viscosity of the cytoplasm. (B) In cellula cotransfection of plasmids that express the 4-bp stem II hhRz within the pUC-VAL and pPrislei scaffolds with plasmid that expresses full-length fix-5'UT human RHO mRNA. Additional comparisons are the inactivated 725 hhRz, 725 hhRzs with upstream tertiary accessory elements (RzB, RzC, RzD). Human RHO mRNA was quantified by real time RT/PCR with hrHO cDNA standardized data comparison. For the pUC-VAL scaffold one-way ANOVA showed significant differences between samples ($P = 0.042$). There was a 49.4% reduction of hrHO mRNA by the active 725 hhRz relative to control ($P = 0.03375$). Catalytic core mutation caused 14.2% reduction of hrHO mRNA but this was not statistically different relative to control or to the active 725 hhRz ($P > 0.05$). In the pUC-VAL scaffold the remaining constructs (RzB, RzC, RzD) did not show significant knockdown of hrHO mRNA relative to control. For the pPrislei scaffold one-way ANOVA showed significant differences among all the samples ($P = 1.92 \times 10^{-5}$). The active 725 hhRz showed 68.4% knockdown of hrHO mRNA relative to control (scaffold alone; $P = 1.36 \times 10^{-6}$). The inactivated 725 hhRz exerted 23.8% knockdown but this was not significantly different from control ($P = 0.17586$). However, the active and inactivated 725 hhRzs showed significantly different knockdown of hrHO mRNA by *t*-test ($P = 4.91 \times 10^{-5}$). All other hhRzs within pPrislei with TAE elements did not achieve significant knockdown of hrHO ($P > 0.05$). (C) Verifying accessibility in the predicted large platform (nts: 653–763) of accessibility in *hrHO* mRNA (*green arrow*). Various hhRzs (*blue arrow*) within the pPrislei scaffold targeted sites both inside (725, 689, 700, 707) and outside (785) the predicted accessibility platform were tested for capacity to cleave *hrHO* mRNA. All targeting sites were GUC↓ cleavage motifs. Reaction conditions used were as in Figure 8A. Cleavage products (*red arrows*) are only present when attacking predicted accessible target sites. Cleavage sites vary in size depending upon the location of the cleavage motif. Inactivating the core of the hhRz prevents cleavage. The noncleaving 785 site is just outside the accessible region but is in one of the most stable regions of the target *hrHO* mRNA fold.

Concurrently, reacting multiple hhRzs to accessible GUC↓ sites within the large accessible region did not enhance the amount of cleavage qualitatively (data not shown), suggesting that steric hindrance (of hhRzs in larger VAI scaffolds) may limit additive attacks of hhRzs within a single accessible region that occupies a limited 3D space in the target mRNA fold. Again, in vitro reactions over 3-hours duration with the hhRz in excess and with nonlimiting Mg^{2+} concentrations (>10 mM) did not lead to complete digestion of the target *RHO* RNA with the maximum product formation was approximately 50%. The extent of cleavage could be impacted by a fraction of the target mRNA in which the 725 cleavage site is inaccessible under these in vitro conditions (Fig. 7B). Based upon all of the above findings, we assigned the R725RzA4.2 hhRz in the VAI-hhRz-2 scaffold (Prislei- δ) as our lead hhRz candidate therapeutic agent.

Recent studies indicate that the ability of hhRz RNAs to form conformations with higher rates of catalytic activity in physiologic conditions of free Mg^{2+} relates to a natural pseudoknot interaction between bases in a tertiary element immediately upstream of the 5' antisense sequence of the hhRz (stem I) and nucleotides in the loop capping stem II of the hhRz proper (e.g., GAAA). The upstream sequences and their structures were deleted from trans hhRz cleavage studies over most of the entire history of their study.^{20,47–54} We confirmed the potential utility of these elements by inserting natural hhRz sequences in cis in the 3'UTR of a SEAP reporter construct.¹⁷ Natural hhRz sequences (including intrinsic targets) from tobacco ringspot (sTRSVd) and peach latent mosaic (PLMVd) viroids containing stem I loop sequences/structures (potential pseudoknot interaction shown with dotted blue line) were much more efficacious than the minimal construct (HH2), which is missing the appropriate stem I loop (Supplementary Fig. S6). sTRSVd exerted approximately 48% SEAP suppression. PLMVd exerted approximately 66% suppression, which was fully reversed by a catalytic core mutation (*G5C*) in the consensus hhRz core, which indicates a bona fide RNA catalytic effect. Replacing the stem I and III recognition sequences of the natural PLMVd hhRz with sequence from our target 725 *RHO* site did not affect the improved knockdown (65%). We also simulated in cis a potential trans acting 725 hhRz with the 725 RzB(cis) construct, where loop I was changed into a bulge. This modification was also successful in retaining an improved knockdown effect

in cis (66%). HhRzs show potent cleavage activities when the substrate is in the same molecule (intramolecular attack) as the hhRz and these enzyme and substrate domains are proximate to one another. These findings encouraged the investigation of use of the upstream TAEs from naturally occurring hhRzs but in the context of therapeutic trans cleavage experiments where the target and enzyme are separate molecules (intermolecular attack).

We made several modifications to our lead 725 trans-acting hhRz to attempt to best incorporate tertiary loop–loop interactions toward enhanced knockdown efficacy based upon prior studies noted above. RzB modification used the PLMVd stem I loop element and PLMVd stem II and loop. RzC modification used a sTRSVd stem I discontinuity and the sTRSVd stem II and loop. RzD modification used a PLMVd stem I discontinuity and the PLMVd stem II loop. Two-dimensional design schematics of these trans constructs are shown (Supplementary Fig. S3). Full-length *hRHO* expression constructs were co-transfected into HEK293S cells with VAI-hhRz chimeras (pUC-VAL [VAI-hhRz-1] and pPrislei [VAI-hhRz-2]) containing hhRzs with these tertiary modifications. QRT-PCR measurements of target mRNA showed that the upstream TAEs (RzB, RzC, RzD) that showed promise in the cis experiments did not enhance *hRHO* knockdown in trans-acting constructs relative to the control 4-bp minimal hhRz structure ($P > 0.05$, $n = 3$) whether these were embedded within the VAI-hhRz-1 or VAI-hhRz-2 scaffolds relative to naive controls (Fig. 8B). The minimal 4-bp stem II 725 hhRz in the VAI-hhRz-2 construct advanced as the lead candidate in our therapeutic pipeline.

A prior study⁵⁵ reported that the addition of an extra nucleotide (A or U) in the minimal hhRz enzymatic core was able to enhance target RNA catalysis against miniature unstructured targets. We attempted to adapt this finding to the 725 hhRz within the VAI-hhRz-2 scaffold. In kinetic in vitro cleavage assays with the short (510 nt) structured *hRHO* RNA substrate we observed no convincing qualitative evidence of enhanced cleavage relative to the control 725 agent (Supplementary Fig. S7). These rational modifications were not tested in cell culture. This approach may be limited by target structure and/or the scaffold itself that supports the hhRz. We also evaluated modulation of the flexibility of the environment around the hhRz within the scaffold by varying the numbers of A's (10 A's on both side or 8 and 7 A's) on both sides of the hhRz within the VAI

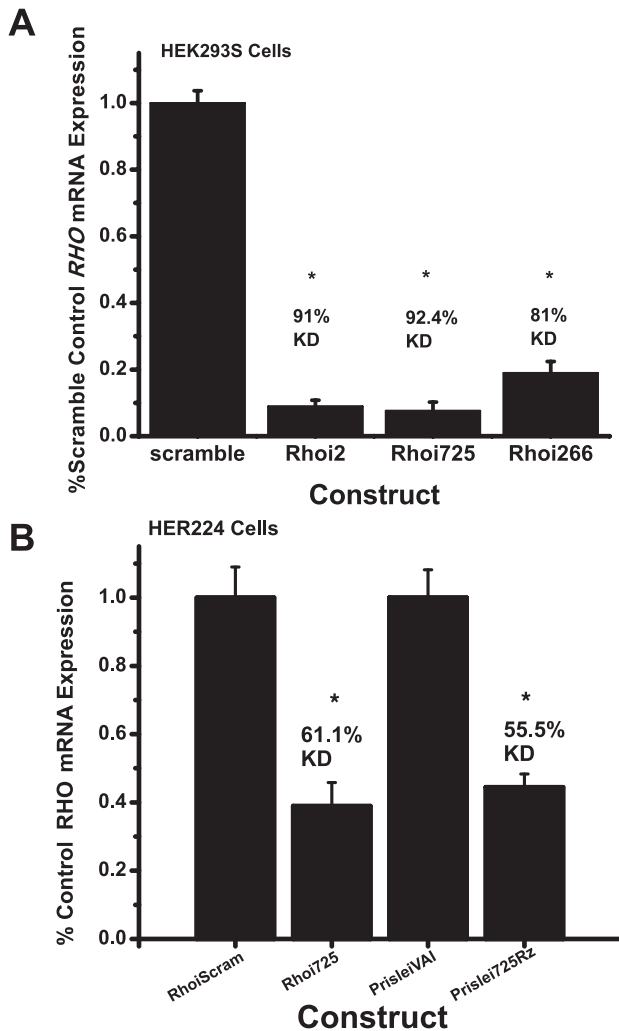


Figure 9. Impact of shRNAs and hhRzs targeting accessible regions of full-length *hRHO* mRNA target in HEK293S cells and HER224 cells. (A) HEK293S cells. shRNA agents were designed targeting *RHO* at the 310 region (*RHOi2*), the 725 region (*RHOi-725*), and the 266 region (*RHOi-266*). The pSUPER expression system was used, and HEK293S cells were transiently co-transfected with pSUPER plasmids along with *pRHO-fix5UT*. Total RNA was extracted from transfected cells 48 hours posttransfection and analyzed for relative *hRHO* mRNA levels using qRT-PCR. Mean percent of control vector (scrambled shRNA) transfection *hRHO* mRNA levels are shown \pm SEM (one-way ANOVA $F = 219.98$, $P = 9.44 \times 10^{-11}$). Asterisks indicate significant ($P < 0.05$) knockdown relative to control transfection. All three RNAi agents showed potent *hRHO* mRNA knockdown compared with scrambled control transfection, with 91.01% knockdown with *RHOi2* ($P = 5.65 \times 10^{-7}$, $n = 4$), 92.39% knockdown with *RHOi-725* ($P = 8.86 \times 10^{-7}$, $n = 4$), and 81.03% knockdown with *RHOi-266* ($P = 3.79 \times 10^{-6}$, $n = 4$). (B) HER224 cells. HER224 cells were transiently co-transfected with plasmids encoding the lead *RHO* 725 human PTGS agents and the *pRHO-fix5UT* plasmid encoding the full-length *hRHO* mRNA transcript. Total RNA was extracted from transfected cells 72 hours posttransfection and analyzed for relative *hRHO* mRNA levels using qRT-PCR. Transfections were carried out in duplicate and

scaffold. These variations did not enhance in vitro activity relative to the standard 5 As, which bound the hhRz in the VAI control constructs (Supplementary Fig. S8).

An attempt was made to enhance cleavage activity at the 725 target site by adapting the stabilizing stem II extensions of the highly active hhRz embedded within the chrysanthemum chlorotic blotch viroid based upon the prior work.⁵⁶ Stem II was extended to 8 or 13 bp in the exact forms of the chrysanthemum hhRz that occur in nature, in the absence of the upstream TAE. Cleavage capacity against the 725-hhRz target site in the short *hRHO* substrate RNA of the chrysanthemum-adapted agent was compared with the 725 hhRz with the minimal 4-bp stem II construct with both agents embedded within the Prislei VAI scaffold (Supplementary Fig. S9). Surprisingly, both naturally occurring forms of the chrysanthemum stem II completely obviated catalytic activity of the minimal hhRz within the VAI scaffold in vitro. Extension of hhRz stem II under all conditions that we have tested appears uniformly and progressively inhibitory with length.

HhRz and shRNA Constructs as Mutation-Independent Therapeutic Agents

We tested if the 725 region of human *RHO* mRNA was amenable to suppression with a shRNA (*RHOi-725*) expressed from extragenic H1 RNA pol-III promoter in the pSUPER plasmid. We also tested a shRNA targeting the region around the 266 codon (*RHOi-266*), a site previously proven amenable to cellular *RHO* mRNA/protein knockdown by PTGS agents,¹⁶ and confirmed in the HTS survey in this study. As a positive control, we used the *Rhoi2* shRNA, which targeted the 310 region in a prior study, which strongly suppressed *hRHO* (94% reduction of protein) in a retinoblast cell culture system.³ The 310 region was also screened by hhRzs in this study, where both the 311 and 320 hhRzs exerted

← assayed in triplicate. Mean percent control vector (scrambled shRNA or VAI without hhRz) transfection *hRHO* mRNA are shown \pm SEM (one-way ANOVA $F = 16.55$, $P = 1.21 \times 10^{-5}$). Asterisks indicate significant ($P < 0.05$) knockdown relative to control vector transfection. Similar to experiments in HEK293S cells, *RHO* 725 PTGS agents showed significant *hRHO* knockdown in disease-relevant cell culture model, HER224 cells. *RHOi-725* suppressed *RHO* by 61.1% compared with scramble control transfection ($P = 5.33 \times 10^{-5}$, $n = 6$). R725RzA4.2 suppressed *RHO* by 55.5% compared with control transfection ($P = 0.003$, $n = 6$).

statistically significant knockdown relative to control but 309 and 316 did not (Fig. 9A). The negative control was an irrelevant scrambled sequence of the same size embedded within the pSUPER plasmid. Co-transfection of all shRNA agents targeted to these accessible regions with full-length *hRHO* construct (p*RHO*-fix5UT) showed potent suppression ($P < 0.05$) of *hRHO* mRNA as measured by qRT-PCR with a standard curve from *hRHO* cDNA (mean knockdown levels: *RHO*i-725, 92.4%; *RHO*i2, 91.1%; *RHO*i-266, 81.0%) relative to control (pSUPER plasmid with scrambled insert) in HEK293S cells (replicates: $n = 4$ for all constructs; Fig. 9A). There were no statistically significant differences in *RHO* suppression in comparisons among the three active shRNAs by both Bonferroni and Tukey tests. The data clearly show that the regions around the 266 and 725 hhRz target sites in full-length *hRHO* are strongly accessible to both hhRz and shRNA annealing and target mRNA suppression. Perhaps not surprisingly, shRNAs, which recruit supportive proteinaceous enzymatic machinery of the RISC system, exert more potent suppression than hhRzs at the same accessible targeting sites, at least in HEK293S cells. We also tested our shRNA and hhRz agents in a retina-derived retinoblast cell line (HER-224), transfecting full-length *hRHO* expression plasmid, and found similar levels of mRNA knockdown for both the hhRz (55.5% knockdown) and shRNA 725 (61.1% knockdown) constructs targeting the 725 region relative to their appropriate control constructs ($n = 6$ replicates for each construct; Fig. 9B). These differences between Prislei-725 and shRNA-725 were not statistically significant ($P = 0.49$) by independent *t*-tests relative to their separate controls in HER224 cells. While there was less sampling in HER224 cells than HEK293S cells, the possibility exists that the performance of PTGS agents could be different in alternative cellular environments.

Finally, we evaluated our lead hhRz and shRNA constructs for use in a MI KD-RECON gene therapy for *hRHO*-linked adRP. An *hRHO* target was “hardened” against the lead 725 PTGS agents by silent, single-base mutations of the 725 and 731 NUH sites that maintained the protein coding sequence. While these simultaneous mutations silently remove hhRz cleavage sites (725 GUC↓ → GUG) or change a more reactive hhRz cleavage site to a less reactive one (UUC↓ → UUU↓), they also change the local structure and decrease the local accessibility of the mRNA as predicted by mppRNA (Fig. 10). Hardening an mRNA target to cleavage is a multivariate

problem that can include not only preclusion of cleavage events, but also the direct accessibility of the annealing platform. When tested experimentally, the hardened *hRHO* mRNA showed significant resistance to both our hhRz and shRNA agents with no significant mRNA or protein knockdown observed compared with scaffold or scrambled controls, respectively. There were significant reductions in WT *hRHO* with the shRNA Rhoi725 construct as follows: 91% mRNA knockdown and 83% protein knockdown (Figs. 11A–C). With the hhRz R725RzA4.2 construct there were also significant but less potent reductions in WT *hRHO*, 59% mRNA knockdown and 59% protein knockdown (Figs. 11D–F). There is a proportional reduction of mRNA and protein with both types of lead agents. The two hardened expression constructs generated mRNAs that were resistant to knockdown by the 725 lead agents promoted strong WT protein expression that was not statistically different from controls. Note that the Rhoi2 shRNA agent, which targets elsewhere in the *hRHO* mRNA, promoted essentially equivalent mRNA knockdown as the Rhoi725 agent against the WT mRNA, and generated equivalent mRNA knockdown with the two hardened WT expression constructs as well. The lead mutation-independent Prislei-725 hhRz agent (targeting 725 GUC↓) also significantly suppressed the *hRHO* mRNA target containing the human *P347S* mutation (CCG to UCG; Fig. 11D). Mutation-dependent hhRz and shRNA agents targeting the site of the *P347S* mutation were unsuccessful (Supplementary Fig. S11); this is likely due to obstructive folding structures around the *P347S* region of the *RHO* mRNA mutant target that limit annealing of the PTGS agent (corroborating).⁵⁷ The mppRNA map shows low accessibility in this region around nt 1135 (see Fig. 4A). A lead 525 hhRz from another group^{6,58} that was also efficacious in our HTS screen was able to suppress *hRHO* mRNA but not as strongly as the 725 lead agent in the same Prislei VAI scaffold (Fig. 11D); this confirms the relative efficacy in the screen of these two agents (see Fig. 5B). These outcomes support the utility of KD-RECON (MI) therapies for *hRHO*-linked adRP and justifies the extensive rational RNA drug discovery undertaken in this study.

Discussion

The genetic heterogeneity of *RHO*-linked adRP necessitates KD-RECON (MI) therapeutic approaches. There are at least 150 mutations in the *hRHO* gene

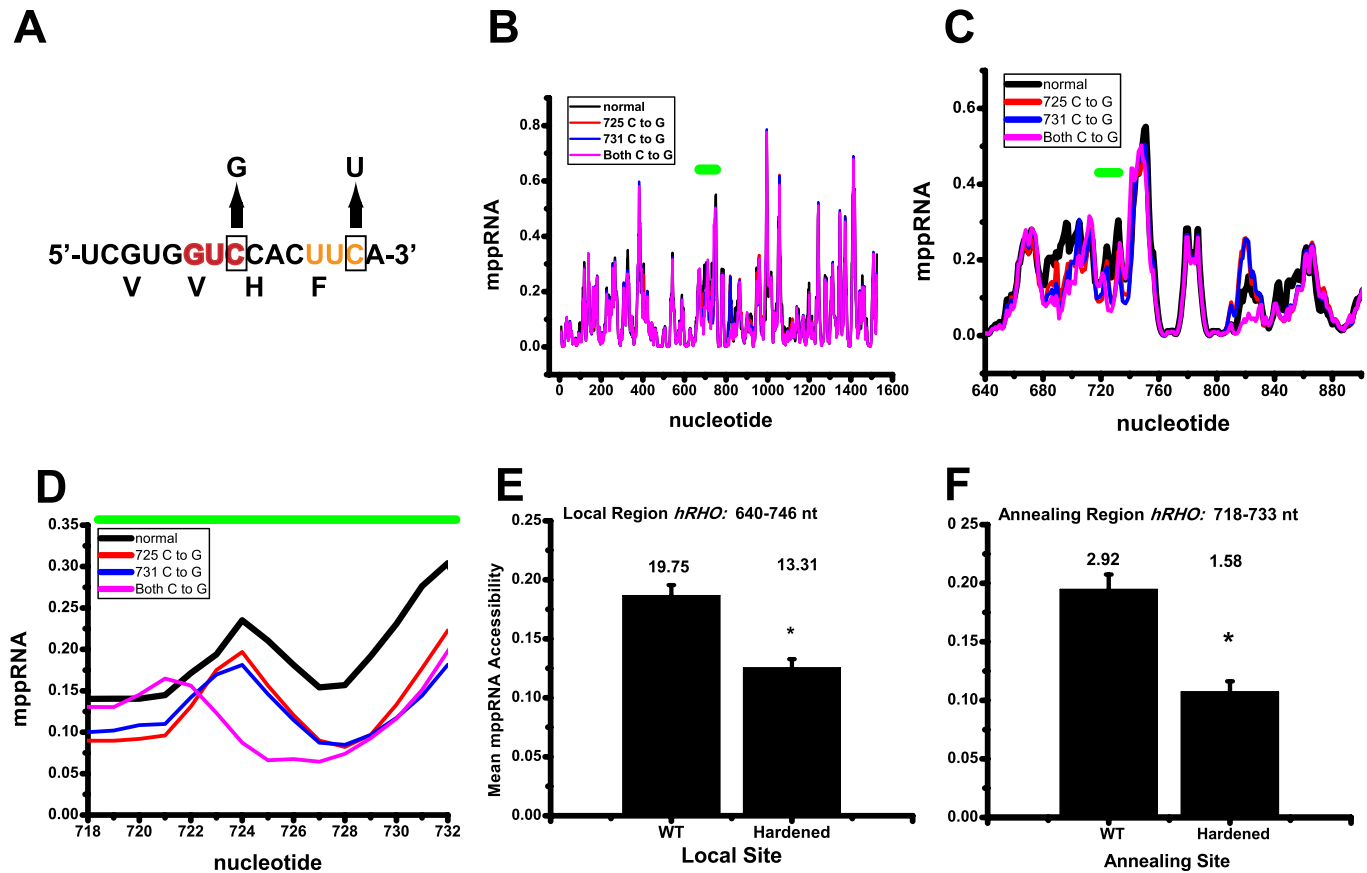


Figure 10. Design of a RECON WT hRHO expression construct. (A) The silent hardening of the *hRHO* WT mRNA occurred by converting the GUC of the 725 cleavage site to the noncleaving GUG which also encodes Valine. The UUC of the 731 cleavage site was silently mutated to UUU, which also encodes phenylalanine, but is a NUH↓ motif that is a poor substrate for hhRz cleavage. (B) The impact of silently hardening the cleavage sites of the 725 or 731 sites on the global mppRNA map relative to the WT *hRHO* mppRNA map. The green bar shows the region of the modifications. The impact of the silent variations occurs only in the immediate region around the 725 targeting site but not beyond. (C) The impact of the silent hardening in the region around the modifications (nts: 640–900). The hardening affects clearly decrease the accessibility in the region around the 725 and 731 cleavage sites and cause some boundary accessibility changes in the local region. (D) The impact of the silent hardening in the annealing region for the 725 hhRz (nts: 718–732). The hardening affects decrease accessibility relative to the WT *hRHO* mRNA. (E, F) Quantitative statistical comparisons of changes in accessibility by hardening. The decrease in the mppRNA accessibility (area under curve) for the regional (E) and local binding site (F) were statistically significant ($P < 0.05$).

that cause inherited retinal degenerations and most of these are single nt mutations that occur in otherwise inaccessible regions of folded mRNA target where PTGS attack is neither rational nor feasible. Moreover, *hRHO* is only one of many genes mutated in ad retinal degenerations (currently 30 identified adRP genes, 15 ad macular degeneration genes, and 10 ad cone or cone rod dystrophy genes in RetNet, in the public domain, <https://sph.uth.edu/Retnet>). To develop PTGS therapeutics for KD-RECON combined gene therapy, two obstacles must be overcome. First, a potent PTGS must be obtained that is active against both WT and mutant mRNA, and a “hardened” replacement gene must be developed that transcribes

an mRNA that is significantly resistant to the lead PTGS agent but still translates adequate levels of WT protein expression to avoid haploinsufficiency and, ideally, to fully reconstitute WT protein levels for normal cellular structure and function. Second, promoter regulatory modules and perhaps other modulatory elements are needed control expression and/or function of both therapeutic and hardened expression constructs. It should be evident that each unique adRP mutant may present a unique systems biology of disease (e.g., time of onset, kinetics of progression) that may require variable knockdown of mutant target (with WT) and variable WT reconstitution. For *hRHO* expression in photoreceptors both

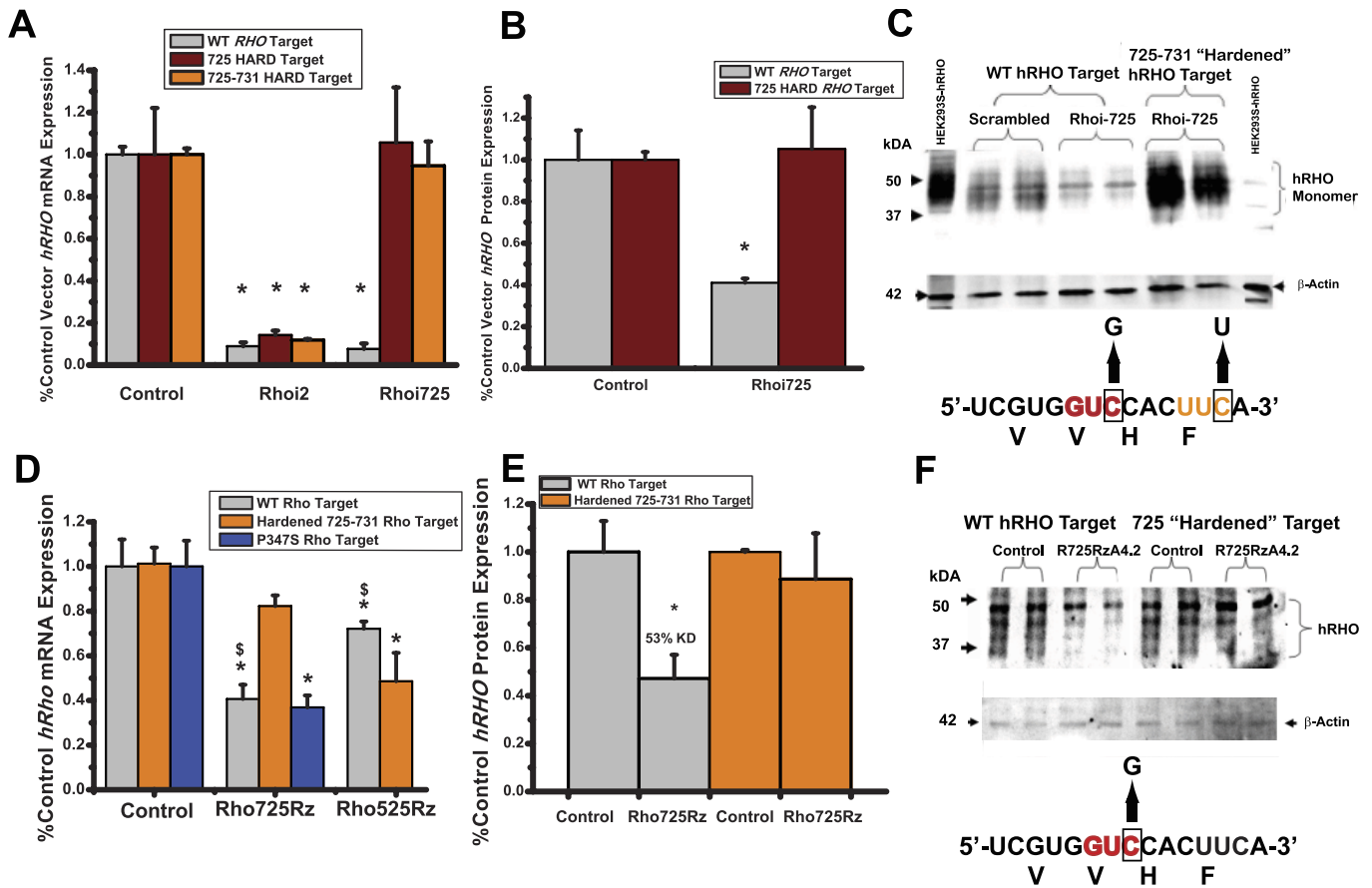


Figure 11. Toward the development of RNA agents for use in preclinical trial of for adRP. HEK293S cells were transiently co-transfected with plasmids encoding PTGS agents and WT target or hardened *hRHO* targets containing either a single silent mutation at the *RHO* 725-hhRz cleavage site (*RHO*-725-HARD) or a double silent mutation at the *RHO* 725 and *RHO* 731-hhRz cleavage sites (*RHO*-725-731-HARD). Total RNA was extracted from transfected cells 48 hours posttransfection and analyzed for relative *hRHO* mRNA levels using qRT-PCR. Cytoplasmic protein was extracted from transfected cells 72 hours posttransfection and analyzed for relative *RHO* protein levels by western blotting. Mean percent control (scrambled shRNA or VAI control) vector transfection *RHO* mRNA or protein levels are shown \pm SEM in bar graphs. Asterisks indicate significant ($P < 0.05$) knockdown relative to control vector transfection. (A) qRT-PCR analysis of *RHO* mRNA levels showed significant resistance of both *RHO*-725-HARD and *RHO*-725-731-HARD constructs to RNAi knockdown by shRNA targeting the *RHO* 725 site (one-way ANOVA $F = 11.29$, $P = 3.29 \times 10^{-7}$). WT *RHO* was knocked down by *RHO*i-725 by 92.39% ($P = 8.86 \times 10^{-7}$, $n = 4$) while both *RHO*-725-HARD and *RHO*-725-731-HARD showed no significant knockdown by *RHO*i-725 ($P = 0.87$, $n = 5$ and $P = 0.67$, $n = 4$, respectively) relative to control. (B) Western blot analysis of *RHO* protein confirmed the observations at the mRNA level, with significant knockdown of WT *RHO* protein by *RHO*i-725 (83.75% knockdown, $P < 0.05$, $n = 2$) and no significant knockdown of *RHO*-725-731-HARD by the same RNAi. *RHO* protein was detected by 1D4 monoclonal antibody, followed by secondary alkaline phosphatase conjugated antibody, and measurement of ECF substrate quantified on a Storm 860 phosphorimager in fluorescence mode relative to β -actin protein levels. (C) The PAGE-SDS gels are shown to the right after immunoblotting. The single-base substitutions in the *RHO* 725 target site are shown below. (D) One-way ANOVA was used to compare knockdown of WT *hRHO* mRNA by Prislei-R725RzA4.2 and Prislei-R525Rz relative to Prislei control ($F = 14.52$, $P = 6.50 \times 10^{-6}$). WT *hRHO* mRNA was knocked down by Prislei-R725RzA4.2 by $59.3 \pm 0.063\%$ ($P = 1.62 \times 10^{-4}$, $n = 22$) and by Prislei-R525Rz by $27.85 \pm 0.032\%$ ($P = 0.037$) relative to control (Prislei alone). Asterisks indicate significance relative to related control. The knockdown by the 725 agent was significantly stronger (31.5% deeper knockdown) than the 525 agent ($P = 1.09 \times 10^{-4}$) ($\$$ indicator over WT bars). For the *hRHO*-725-HARD target testing by hhRzs, the ANOVA test showed significant differences among constructs ($F = 7.68$, $P = 0.00359$). For the *hRHO*-725-HARD there was no significant knockdown by R725RzA4.2 ($P = 0.13$, $n = 4$) relative to control. With the *hRHO*-725-HARD there was significant knockdown by the Prislei-R525Rz ($P = 0.002$), which is expected as this targets a different region, which is not altered in this hardened mRNA. The Prislei-R725RzA4.2 agent was able to significantly reduce mutant P347S *hRHO* mRNA in cells ($63.09\% \pm 0.05\%$) relative to Prislei control ($P = 5.73 \times 10^{-4}$). In a separate *t*-test comparison the Prislei-R725RzA4.2 did not exert significantly different knockdowns of the WT *hRHO* versus the P347S *hRHO* mRNAs ($P = 0.77$). (E) Western blot analysis of *RHO* protein confirmed the observations at the mRNA level, with significant knockdown of WT *RHO* by R725RzA4.2 (60.0% knockdown, $P < 0.05$, $n = 2$) and no significant knockdown of *RHO*-725-HARD by the same hhRz. (F) The PAGE-SDS gels are shown to the right after immunoblotting. The single-base substitution in the *RHO* 725 target site is shown below.

underexpression and overexpression of the WT protein can lead to photoreceptor demise.^{59–65} Therefore, regulation of expression and function of both the therapeutic PTGS agent and the WT hardened mRNA may be critical to a broad range of therapeutic coverage for diverse *hRHO* adRP mutations.

Development of potent PTGS agents presents the immediate challenge of the complex structure, biochemistry, and cell biology of the target mRNA, as well as the structure, function, and dynamics of the therapeutic agents themselves. Target mRNAs are folded into dense secondary and tertiary structures, are coated with heterogeneous proteins (e.g., hnRBP A), and reside in diverse intracellular compartments with distributed lifetimes. All of these factors strongly constrain the second-order kinetic interaction of target mRNA with a smaller PTGS ligand. To succeed in this challenge, one is best served by first identifying large, stable, accessible regions of the target within the cellular milieu at physiologic temperature. We developed a screening platform where *in silico* computational tools and *in vitro* experimental tools allow us to rapidly identify stable accessible sites in the target mRNA for efficient annealing by hhRz or shRNA PTGS agents.¹⁷ Here, we used this HTS platform to identify lead candidate hhRz and shRNA agents against full-length *hRHO* mRNA target. A bicistronic SEAP-reporter fusion RNA construct allows for rapid, systematic testing of candidate sites in a cell culture system to determine the optimum PTGS target site and identify a lead candidate agent for further optimization.¹⁷

Robust mRNA Target Accessibility Determinations

With an in-house bioinformatics model (mppRNA) to predict accessibility within arbitrary target mRNAs, we mapped regions of accessibility and inaccessibility in *hRHO* mRNA. We integrated the area under the peaks in the accessibility map to generate rank-ordered weights as a first step prior to identifying ubiquitous NUH↓ cleavage sites. mppRNA uses three algorithms (MFold, SFold, OW) and we sought locations of regions of accessibility mapped by all three approaches (intersection of the vector accessibility sets), currently using equivalent weighting of the three outputs and the assumption of independence. Further effort is ongoing to attempt to weight the individual vectors in the model for other target mRNAs of relevance to gene therapy

(unpublished data). We tested accessibility at predicted sites using the experimental MAST approach, but redesigned in our hands to be gene-specific (gsMAST). GsMAST confirmed regions of accessibility and inaccessibility identified by *in silico* testing. GsMAST is simple to perform as an experimental approach and provides enhanced confidence that the *in silico* mapping by mppRNA is valid for a given target. It does not, however, identify regions that could be accessible, but which were not identified by mppRNA. This issue could be resolved by developing a rich gsMAST discrete tag library that covers the entire target mRNA to avoid the biased mppRNA sampling; this would require approximately 1515 unique gsMAST ODNs to cover a 1532-nt *hRHO* mRNA. In contrast, cMARS is a combinatorial approach that seeks the intersection of an accessible region of a target mRNA that contains NUH↓ cleavage sites. It is not biased by the need for predetermination of likely accessible sites by *in silico* mapping. cMARS clearly identified accessible regions around the 725 and 266 cleavage sites (top leads) and also showed that the mRNA target is largely inaccessible to most small ligand attacks, confirming that the true accessible space in a folded mRNA is of low probability. cMARS will be described in detail elsewhere (unpublished data). When we compared the weight of accessible regions to the extent of SEAP suppression in the HTS there was a good and significant correlation further substantiating the expanded use of mppRNA to map accessibility of arbitrary target mRNAs for testing of therapeutic PTGS designs. It should be mentioned that high-resolution, single-nt accessibility maps can be obtained by selective 2-hydroxyl acylation analyzed by primer extension (SHAPE) mapping, although the approaches described here are simpler but provide a less resolved averaged perspective sampled by conformational windows (15 nt) or probing ODNs.⁶⁶

We examined the functional relationship of knockdown of target with mppRNA predictions of local accessibility of the exact annealing platform of the target or the integrated peak area in the accessibility plot (Figs. 6A, 6B). The statistical linear regressions are taken through the origin (origin is defined as $x = 0$, $y = 0$), rationally, because the control construct has no knockdown (y -axis) and no meaningful predicted accessibility (x -axis) if there is no means to anneal to the target mRNA. The fit is strong for the relationship of knockdown to integral of the local accessibility peaks even though a single peak weight can cover multiple NUH↓ target sites ($R^2 = 0.88$; Fig. 6A). The

fit of knockdown to the area under the mppRNA accessibility curve under each target annealing site (15 mer) is weaker ($R^2 = 0.66$; Fig. 6B). There are several points to make. First, local accessibility of (average) integrated area of the target may be more important to knockdown than the immediate antisense annealing site platform. The cleavage reaction presumes that the annealing reaction has completed. The annealing reaction depends upon a second-order reaction in solution phase between the target mRNA annealing platform and the therapeutic RNA, in particular the antisense flanks of the hhRz. A second-order reaction is, by nature, dependent on the concentrations of the two interacting molecular species, which dictate a biophysical collision frequency that specifies the probability of interaction. The probability of annealing is dependent upon the collision frequency, the concentrations of reactants, the accessibility of the local target annealing platform, the accessibility of the antisense flanks of the hhRz, and the orientational (vectorial) approach in the collisions. At least, the lack of accessibility of the annealing platform of the target, lack of accessibility of the antisense flanks of the hhRz, insufficient concentrations in the co-localized regions of cellular space, or buried versus surface annealing platforms of the target relative to the size or volume of the ribozyme in the scaffold could affect PTGS outcomes. The average effect obtained by integrating the peak weight may more reliably reflect conditions that enhance the full annealing probability, perhaps by enhancing kissing complex formation prior to the annealing event at the specific target platform.

Second, another factor may be that mppRNA, as currently calculated, may not yet be fully optimized to predict local accessibility of the target mRNA. That we are able to have some degree of prediction, at least to identify highly accessible sites (the 653–763 region), is a significant step forward, and could guide development of PTGS agents to arbitrary targets. Currently, the weighting factors for the vectors of the three algorithms (MFold, SFold, OW) are all set arbitrarily to 1.0 (equal), but this has not been tested or confirmed on a substantial set of target mRNAs for which larger data sets (multiple experimentally tested target sites where knockdown of target is assessed in cells) are available. Correlation might be better if the weighting factors are not uniform. As part of ongoing work, we have identified a small ensemble of studies (this one included) that provide such substantial cellular knockdown data sets across a number of potential cleavage sites (e.g., NUH↓) and

have begun a multiple variable linear regression study. But, optimization of mppRNA is not the focus of the current study. Third, there may be additional computational variables that could contribute to an assessment of accessibility (e.g., 3D RNA folding). As suggested above, the 3D shape of the target accessibility platform, its location in the target (on the surface or buried), and the 3D size of the therapeutic RNA and the shape of its antisense flanks could all influence the probability of annealing. The predicted 3D images of local target annealing sites (Figs. 6D, 6E; Supplementary Figs. 10A, 10B) clearly show the potential complexity of this process. In summary, the mppRNA (version 1) as it currently stands directed us to lead candidates for hRHO that are valuable for further therapeutic development. It is a solid beginning, but further optimization may be possible as we better understand the variables and can potentially model such processes.

Large RNA Molecule PTGS “HTS” Screen

Exploiting fusion RNA approaches we identified ways of conducting screens of PTGS agents expressed in cultured human cells.¹⁷ Here, we conducted the screen for full-length *hRHO* using a stable cell line expressing the bicistronic mRNA *hRHO*-IRES-*SEAP*. With the *hRHO* component upstream of the IRES the intended target is able to begin folding into native structures as these emerge from RNA polymerase II, and the IRES (for cap-independent translation of *SEAP*) acts as an insulator to separate folding of the upstream target from the downstream *SEAP* reporter component. This makes it more likely that the target component of the bicistronic mRNA will reflect structures and accessibility relevant to the properties of the full-length independent mRNA (without IRES-*SEAP* elements attached) when attacked by PTGS agents. With highly efficient, positively selected PTGS plasmid construction approaches developed in this lab, we are able to produce large sets of plasmid-based PTGS agents to test for rank-order efficacy. This approach is scalable by at least two log-orders with robotic approaches, which would readily cover the full number of NUH↓ sites in most mRNA targets. The novel tools and technology platform that we established here greatly enhances our ability to identify lead candidate RNA biologics (PTGS agents) to arbitrary disease target mRNAs.

Using our rational design and cellular efficacy screening approach, we identified a novel region in *hRHO* mRNA that is the very sensitive to hhRz cleavage. The 725-hhRz site appears to be the

optimum locale in this target for design of knock-down PTGS agents to be used for intracellular cleavage. The 725 region is clearly the most heavily weighted accessible region by in silico mppRNA mapping, and was further confirmed experimentally by gsMAST and cMARS. In vitro hhRz cleavage assays in the VAI-hhRz-2 scaffold clearly showed that multiple GUC↓ cleavage sites were accessible to binding and cleavage in the large region (positions: 653–763) of full-length *hRHO* mRNA. The two optimum 725 GUC↓ and the 731 UUC↓ cleavage sites identified in the screen are within the large span of accessibility. The 266 CUC↓ cleavage site was third in rank order in the screen for knockdown, and was also shown previously by this lab to support hhRz knockdown in cells.¹⁶ The ribozymes targeting the lead 725 GUC↓ site were further optimized in preparation for preclinical testing.

HhRz Optimization

The 6-bp stem II 725 hhRz in the VAI-hhRz-1 scaffold from the HTS, when tested against full-length human *RHO* in co-transfection experiments exerted significant mRNA knockdown (28%) but the catalytic core mutation failed to cause full reversal of suppression. We interpreted this result as an inhibitory effect of extensions of stem II on the catalytic function of the hhRz enzyme core.⁴⁴ This hypothesis is rational in that upon full annealing of the hhRz to the target, the hhRz must undergo conformational changes in order to achieve an atomic level alignment of nucleotide residues essential to formation of the active state complex on the mechanistic pathway to the cleavage event.⁵⁴ Any energetic or structural barrier is likely to inhibit the (Arrhenius) rate of transition over the activation energy barrier into a catalytically active state. One can further hypothesize that any factor that influences the ability of the hhRz to undergo conformational changes once bound to the target could limit the cleavage event or its overall efficacy. Such conformational restrictions (decreases in entropy) could come from either hhRz folding itself (e.g., stem II stabilization in a minimal hhRz) or the scaffold boundary conditions. In the screen we embedded the hhRzs in a 49-nt harbor predicted to be single stranded without an embedded hhRz (see Fig. 2A). This harbor caps a GC rich stem. It possible that some of the antisense sequences of the hhRzs tested or the common core hhRz itself could have interacted by Watson-Crick base pairing with the nt constituting the harbor. And, there was no design effort to add flexibility to the boundary between the

hhRz and the scaffold harbor in VAI-hhRz-1, although there was ample sequence space in the 49-nt harbor designed intentionally for flexibility. When we placed the minimal hhRz 725 with a standard 4-bp stem II capped by a GAAA tetraloop into the VAI-hhRz-1 scaffold, we saw an increase in catalytic performance (to ~50% mRNA knockdown) and a full reversal of knockdown activity by catalytic core inactivating mutation. This showed that the extended stem II of the minimal hhRz was inhibiting the cleavage potential of the enzyme, whereas the antisense flanks (and annealing energy) were otherwise identical between the two ribozymes. The inhibitory effects of stem II extension are also shown through our experiments with the chrysanthemum hhRz stem II constructs (8 or 13 bp) that completely inhibited hhRz catalysis. These outcomes suggest a way to modulate hhRz activity through variation in stem II length.

We tested a variety of upstream tertiary accessory elements to try to drive catalytic active state transitions for the minimal 725 hhRz with 4-bp stem II region within the VA scaffolds. Within the VAI-hhRz-1 scaffold (pUC-VAL) none of the tertiary elements tested (B, C, D) exerted greater knockdown than the minimal 725 hhRz (4-bp stem II). A subsequent VAI scaffold (VAI-hhRz-2, pPrisei) was designed for testing and comparing hhRz 725 activity. This version of the VAI scaffold, modeled after a prior study,³⁵ removed the large hhRz harbor and the GC-rich stem leaving only a bulge loop for hhRz ligation and relatively more flexible boundary conditions with five A residues on each side of the hhRz. Within this simpler scaffold the minimal 725 hhRz activity showed some enhanced relative to activity within the VAI-hhRz-1 scaffold at both the in vitro cleavage assay level and in cultured cells. Moreover, catalytic activity was fully reversed with enzyme core mutations. However, addition of upstream tertiary accessory elements again failed to enhance cellular knockdown with full-length *hRHO* mRNA in the VAI-hhRz-2 scaffold (Prisei-VAI). The catalytic enhancement by these upstream elements, which occurred when the target was in cis with respect to the hhRz were lost (in both VAI scaffolds) in trans. It should be noted that the naturally occurring tertiary accessory elements from PLMVd and TRSVd have greatest reported impact when tested against miniature substrates.⁵³ The roles of the highly stable VAI RNA structure, or the presence of an arbitrary constraining scaffold on the activity of the TAEs or hhRz activity in general are unknown. The 4-bp stem

II classical hhRz (RzA4) model in our second VAI RNA chimera (VAI-hhRz-2, pPrislei) was designated our lead candidate as the most kinetically active construct.

On shRNA Therapeutics Targeting HhRz-Active Regions

shRNAs targeting 725 and 266 regions demonstrated potent log-order (>90%) knockdown of target mRNAs in cellula in HEK293S cells. shRNA suppression was greater than the hhRzs targeting the same regions. This is not surprising given that RNAi uses protein-based catalysis of the RNA-induced silencing complex to cleave target mRNAs whereas hhRzs do not use cellular protein support and are solely dependent upon structure-dependent RNA nucleotide chemistry. While the potency for RNAi agents is generally greater than hhRzs, shRNAs require only a “seed” sequence of approximately 7 nt for functionality, which is the major reason for the often reported off-target effects of RNAi in the therapeutic context.^{67–71} RNAi evolved to modulate the expression of large sets of mRNAs. HhRzs in this study, and commonly in other studies, use 6 to 7 nt for each antisense flank sequence creating a total hybridization span of 12 to 14 nt.⁷² This extent of Watson-Crick complementarity is necessary to maintain target annealing during the generally slow enzyme kinetics of the hhRz (~1/min).^{73,74} With 12 to 14 nt of antisense span needed for hhRz functionality there is substantially greater specificity for the intended target in the (e.g., human) transcriptome than an RNAi agent. Hence, while the potency may be greater (currently) for shRNAs, the efficacy/toxicity ratio of hhRzs relative to shRNA are likely to be greater in a therapeutic context. However, we did not observe significant differences in PTGS between the 725 shRNA and the Prislei-724 hhRz in HER224 retina-derived cells. The hhRz performance was similar in the two cell types, but the shRNA knockdown was greater in HEK293S cells. The finding that shRNA performance could be cell-type dependent raises additional questions of its therapeutic utility. Having made this point, there is clearly room for improvement of hhRz potency. shRNAs targeting a particular accessible site in a target mRNA may establish a limit on the potential potency of hhRzs at that site. shRNAs require accessibility as well, which is proven by the testing of both shRNA and hhRzs as mutation-dependent agents for the P347S *hRHO* mRNA; neither agent exerted signifi-

cant knockdown, as expected for an inaccessible region of the target mRNA fold that does not immediately support PTGS annealing. For all PTGS agents (antisense, ribozyme, shRNA), accessibility of the mRNA is a precondition for strong knockdown suppression.

Cellular Testing in the Context of Mutation-Independent PTGS Therapeutics

The KD-RECON (MI) strategy for ad mutations in a gene-causing monogenetic hereditary retinal or ocular degeneration requires the identification of a lead knockdown PTGS agent, which can be used with most or all known mutations (suppresses mutant and WT mRNA/protein) and a “hardened” mRNA, which cannot be cleaved by the therapeutic but that reconstitutes target protein expression to avoid haploinsufficiency. We tested our lead hhRz agent against our hardened *hRHO* target mRNA, which was designed under considerations of both the reactivity of the NUH↓ site and engineered changes in the accessibility of the annealing or local region of targeting. Mutations in the “hardened” *RHO* targets demonstrated resistance to lead agent PTGS knockdown. Significantly, only two single-base, silent mutations were necessary to achieve essentially complete resistance of our “hardened” *RHO* target. Computational analysis of our designer “hardened” targets showed a significant change in local secondary structure introduced by the silent mutations that likely impact accessibility of the region to annealing by our PTGS agents in addition to the resistance due to the loss of hhRz cleavage sites (Fig. 10).

One might consider that primary sequence homology of our candidate 725 annealing site within rod opsin mRNAs of several mammals offers potential for testing our successful and optimized PTGS agents in small- and large-scale models. However, the comparison of primary sequences of various mammalian targets does not guarantee equivalent accessibility at a given region of homology, which is the critical issue for therapeutic transfer compatibility (Trujillo AJ, et al. *IOVS* 2017;58:ARVO E-Abstract 4493). A critical feature for broad utility of a single MI PTGS agent is that the many mutations in a single gene that cause inherited retinal degeneration should not affect the accessibility at the single-target cleavage site for the PTGS agent site; a recent deep bioinformatics *hRHO* RNA folding study from this lab shows that the 725 target site accessibility is not quantitatively impacted by over 90% of known *hRHO*

mutations.²⁸ This supports potential large scale use of the 725 PTGS agent for *hRHO* adRP. Here, we demonstrated a generic computational/experimental strategy that can be broadly used to realize strong RECON hardened target expression constructs.

Comparison of Lead Agents to PTGS Agents From Other Studies

We compared our hhRz MI lead agent(s) to prior lead hhRzs (485, 525),⁶ which gave a partial rescue effect in a rat model of adRP that expressed a mouse *P23H* mutant *RHO* gene, and more recently a partial rescue in a canine T4R *RHO* model of adRP.⁵⁸ Our 725-hhRz lead, in the adenoviral VAI scaffold chosen, is more potent than the 525 hhRz at *hRHO* mRNA suppression in cultured cells. As the set of available agents have not been compared head-to-head in an appropriate animal model, the best agents for greatest protection in patients are yet to be identified. Our efforts are directed to optimization of the existing lead agent developed in our hands (725 hhRz), to achieve the most potent agent, which has the greatest and most persistent effect in humanized animal models of adRP. Our shRNA targeting the 725 region shows similar knockdown potential (~1 log order) against *hRHO* mRNA when compared to other reported agents,^{3,4} and to a more recently identified shRNA.⁵⁸ In the recently reported dog adRP study, the dose of AAV with the 525-hhRz expression construct had to be so high to induced adequate knockdown of the target that it induced toxicity in the outer retina, and hhRzs were dropped from the study design.⁵⁸ Our lead 725 hhRz was identified in a screen that involved tests of the 525 hhRz in the same VAI scaffold (Fig. 5A) and the 725 agent performed with deeper knockdown, which was confirmed in independent measures in a more refined Prislei VAI scaffold (Fig. 11D). The improved knockdown performance of the 725 hhRz versus the 525 hhRz, as measured in this study, could support hhRz utility in gene therapeutic applications for *hRHO* adRP. If hhRz agents can be improved beyond that already achieved and reported here, then hhRzs will clearly have therapeutic potential to treat human diseases.

Comparison of Ribozyme to shRNA Knockdown

All PTGS agents (ribozyme, antisense, RNAi) require accessibility of the target to manifest annealing-dependent knockdown and none have apparent intrinsic RNA helicase activity to unwind

pre-existing structures. It is increasingly clear that the potency or efficacy of knockdown by an expressed shRNA is commonly greater than that of a ribozyme targeting the same accessible region of a target mRNA. This is not surprising as the RISC only uses the RNA guide strand to target the complexed proteinaceous endonuclease (Ago2) to the cleavage site, whereas the ribozyme accomplishes RNA cleavage solely with properly structured RNA nt-mediated chemistry to accelerate the reaction. Even though the ribozyme-mediated knockdown of target mRNA in human cells at the 725 site is strong (50%–65%), shRNAs add an additional 20% to 30% target suppression in the HEK293S system. Ribozymes offer substantially greater specificity than shRNAs because of the greater extent of the antisense flanks needed for functionality (12–14 nts for the hhRz versus 6- to 7-nt seed sequences for the shRNA). The off-target effects of shRNAs are anticipated to be much greater than for ribozymes, in part because this is how RNAi evolved to regulate the expression of many genes in a given systems biology. It is expected that a single shRNA or miRNA regulates up to 100 or more genes in mammals. Toxicity could clearly result from plethora of such off-target effects because the fundamental systems biology is altered by the therapeutic. Hence, ribozymes are expected to have substantially greater efficacy/toxicity ratio than shRNAs. The relative benefit ribozymes in the therapeutic context may be substantially enhanced if approaches can be identified to collapse the potency differential with RNAi at a known accessible region. Approaches to this scientific challenge can be both rational and evolutionary and are an ongoing effort of this laboratory. Important structural and functional lessons about ribozymes were learned after the boom of RNAi (which caused many therapeutic ribozyme investigators to leave the field), and these and other more recent lessons could clearly influence a revitalization of this therapeutic modality.^{75–77}

Conclusions

Combining mRNA accessibility determination methods and a cell-based efficacy screen, we identified a lead accessible site (725) for a strongly expressed *hRHO* mRNA. The lead candidate hhRz-targeting 725 site was embedded in a highly expressed and structured viral RNA scaffold (engineered adenoviral VAI) that traffics efficiently from the nucleus to the cytoplasm. Optimized versions of hhRz targeting this 725 site, and hardened targets to

reconstitute WT target protein expression, provide a candidate mutation-independent gene therapy platform for ad retinal degenerations caused by mutations in the *hRHO* gene. These agents are currently being tested in humanized models of *RHO* adRP, which express mutant and WT *hRHO* genes in mouse photoreceptors. The robust approach outlined in this article is extendable to the development of knock-down PTGS agents against any arbitrary validated mRNA target that go well beyond our initial context of ad disease. The same agents could be used against WT *hRHO* mRNA when RHO reduction is a viable therapeutic strategy (e.g., age-related macular degeneration). The same process could be used against an arbitrary mRNA target where a knockdown approach is a valid strategy for therapeutics in any disease state.

Acknowledgments

The authors thank Gregory Wilding, PhD, Professor and Chair of the Department of Biostatistics, University at Buffalo, School of Public Health and Health Professions, with whom we discussed the application and use of statistical models in this manuscript and the concepts of how to represent variance. This manuscript is dedicated to the memory of Richard T. Sullivan, an informal astronomer, who initiated and helped evolve the scientific interests of the corresponding author. This approach to hhRz and shRNA screening is also described in a US Patent (US Patent 8252527, Method for identification of polynucleotides capable of cleaving target mRNA sequences, 2012).

Supported by grants from the National Eye Institute award (R01 EY013433, JMS: PI), a VA Merit Award (1I01BX000669, JMS: PI) from the United States Department of Veterans Affairs (Biomedical Laboratory Research and Development Service), a SUNY Health Now award (JMS Organizing PI), a Research to Prevent Blindness Unrestricted Grant (to the Department of Ophthalmology at the University at Buffalo), and an Oishei Foundation (Buffalo, NY) grant to the Department of Ophthalmology at University at Buffalo. This work was conducted at, and supported in part, by facilities and resources provided by the Veterans Administration Western New York Healthcare System. The contents do not represent the views of the Department of Veterans Affairs or the US Government. Jack M.

Sullivan, MD, PhD, is employed as a Staff Physician at the VA Western NY Healthcare System, Buffalo, NY, and as a Professor of Ophthalmology at the University at Buffalo.

Disclosure: **E.H. Yau**, P; **R.T. Taggart**, None; **M. Zuber**, None; **A.J. Trujillo**, None; **Z.S. Fayazi**, None; **M.C. Butler**, None; **L.G. Sheflin**, None; **J.B. Breen**, None; **D. Yu**, None; **J.M. Sullivan**, (P)

References

1. Millington-Ward S, O'Neill B, Tuohy G, et al. Strategems in vitro for gene therapies directed to dominant mutations. *Hum Mol Genet.* 1997;6: 1415–1426.
2. Sullivan JM, Pietras KM, Shin BJ, Misasi JN. Hammerhead ribozymes designed to cleave all human rod opsin mRNAs which cause autosomal dominant retinitis pigmentosa. *Mol Vis.* 2002;8: 102–113.
3. Cashman SM, Binkley EA, Kumar-Singh R. Towards mutation-independent silencing of genes involved in retinal degeneration by RNA interference. *Gene Ther.* 2005;12:1223–1228.
4. O'Reilly M, Palfi A, Chadderton N, et al. RNA interference-mediated suppression and replacement of human rhodopsin in vivo. *Am J Hum Genet.* 2007;81:127–135.
5. O'Reilly M, Millington-Ward S, Palfi A, et al. A transgenic mouse model for gene therapy of rhodopsin-linked retinitis pigmentosa. *Vision Res.* 2008;48:386–391.
6. Gorbatyuk M, Justilien V, Liu J, Hauswirth WW, Lewin AS. Preservation of photoreceptor morphology and function in P23H rates using an allele independent ribozyme. *Exp Eye Res.* 2007; 84:44–52.
7. Kiang AS, Palfi A, Ader M, et al. Toward a gene therapy for dominant disease: validation of an RNA interference-based mutation-independent approach. *Mol Ther.* 2005;12:555–561.
8. Palfi A, Ader M, Kiang AS, et al. RNAi-based suppression and replacement of rds-peripherin in retinal organotypic culture. *Hum Mutat.* 2006;27: 260–268.
9. Sullivan JM, Yau EH, Kolniak TA, Sheflin LG, Taggart RT, and Abdelmaksoud H. Variables and strategies in development of therapeutic post-transcriptional gene silencing agents. *J Ophthalmol.* 2011;2011:531380.
10. Lieber A, Strauss M. Selection of efficient cleavage sites in target RNAs by using a ribozyme

- expression library. *Mol Cell Biol.* 1995;15:540–551.
11. Scherr M, Rossi JJ. Rapid determination and quantitation of the accessibility to native RNAs by antisense oligodeoxynucleotides in murine cell extracts. *Nucleic Acids Res.* 1998;26:2455–2461.
 12. Kretschmer-Kazemi F, Szakiel, G. The activity of siRNA in mammalian cells is related to structural target accessibility: a comparison with antisense oligonucleotides. *Nucleic Acids Res.* 2003;31:4417–4424.
 13. Brown K, Chu C, Rana T. Target accessibility dictates the potency of human RISC. *Nat Struct Mol Biol.* 2005;12:469–470.
 14. Sullivan JM, Yau EH, Taggart RT, Butler MC, Kolniak TA. Bottlenecks in development of retinal therapeutic post-transcriptional gene silencing agents. *Vision Res.* 2008;48:453–469.
 15. Sullivan JM, Yau EH, Taggart RT, Butler MC, Kolniak TA. Relieving bottlenecks in RNA drug discovery for retinal diseases. *Adv Exp Med Biol.* 2012;723:145–153.
 16. Abdelmaksoud HE, Yau EH, Zuker M, Sullivan JM. Development of lead hammerhead ribozyme candidates against human rod opsin mRNA for retinal degeneration therapy. *Exp Eye Res.* 2009;88:859–879.
 17. Yau EH, Butler MC, Sullivan JM. A cellular high-throughput screening approach for therapeutic trans-cleaving ribozymes and RNAi against arbitrary mRNA disease targets. *Exp Eye Res.* 2016;151:236–255.
 18. Amarzguioui M, Prydz H. Hammerhead ribozyme design and application. *Cell Mol Life Sci.* 1998;54:1175–1202.
 19. Birikh KR, Heaton PA, Eckstein F. The structure, function and application of the hammerhead ribozyme. *Eur J Biochem.* 1997;245:1–16.
 20. Uhlenbeck OC. A small catalytic oligoribonucleotide. *Nature.* 1987;328:596–600.
 21. Haseloff J, Gerlach WL. Simple RNA enzymes with new and highly specific endoribonuclease activities. *Nature.* 1988;334:585–591.
 22. Hannon GJ. Interference. *RNA Nature.* 2002;418:244–251.
 23. Caplen NJ, Parrish S, Imani F, Fire A, Morgan RA. Specific inhibition of gene expression by small double-stranded RNAs in invertebrate and vertebrate systems. *Proc Natl Acad Sci U S A.* 2001;98:9742–9747.
 24. Caplen NJ. RNAi as a gene therapy approach. *Expert Opin Biol Ther.* 2003;3:575–586.
 25. Sullivan LS, Bowne SJ, Birch DG, et al. Prevalence of disease-causing mutations in families with autosomal dominant retinitis pigmentosa: a screen of known genes in 200 families. *Invest Ophthalmol Vis Sci.* 2006;47:3052–3064.
 26. Sullivan LS, Bowne SJ, Reeves MJ, et al. Prevalence of mutations in eyeGENE probands with a diagnosis of autosomal dominant retinitis pigmentosa. *Invest Ophthalmol Vis Sci.* 2013;54:6255–6261.
 27. Daiger SP, Bowne SJ, Sullivan LS. Genes and mutations causing autosomal dominant retinitis pigmentosa. *Cold Spring Harb Perspect Med.* 2015,5:a017129.
 28. Froebel BF, Trujillo AJ, Sullivan JM. Effects of pathogenic variations in the human rhodopsin gene (*hRHO*) on the predicted accessibility for a lead candidate ribozyme. *Invest Ophthalmol Vis Sci.* 2017;58:3576–3591.
 29. Nathans J, Hogness DS. Isolation and nucleotide sequence of the gene encoding human rhodopsin. *Proc Natl Acad Sci U S A.* 1984;81:4851–4855.
 30. Zuker M. Mfold web server for nucleic acid folding and hybridization prediction. *Nucleic Acids Res.* 2003;31:3406–3415.
 31. Ding Y, Chan C, Lawrence C. Sfold web server for statistical folding and rational design of nucleic acids. *Nucleic Acids Res.* 2004;32:W135–W141.
 32. Mathews DH, Burkard ME, Freier SM, Wyatt JR, Turner DH. Predicting oligonucleotide affinity to nucleic acid targets. *RNA.* 1999;5:1458–1469.
 33. Popena, M., Szachniuk, M., Antczak, et al. Automated 3D structure composition for large RNAs. *Nucleic Acids Res.* 2012;40:e112.
 34. Zhang HY, Mao J, Zhou D, et al. mRNA accessible site tagging (MAST): a novel high throughput method for selecting effective antisense oligonucleotides. *Nucleic Acids Res.* 2003;31:e72.
 35. Prislei S, Buonomo SM, Michienzi A, Bozzoni I. Use of adenoviral VAI small RNA as a carrier for cytoplasmic delivery of ribozymes. *RNA.* 1997;3:677–687.
 36. Brummelkamp TR., Bernards R, Agami R. A system for stable expression of short interfering RNAs in mammalian cells. *Science.* 2002;296:550–553.
 37. Nathans J, Weitz CJ, Agarwal N, Nir I, Papermaster DS. Production of bovine rhodopsin by mammalian cell lines expressing cloned cDNA: spectrophotometry and subcellular localization. *Vision Res.* 1989;29:907–914.
 38. Stillman BW, Gluzman Y. Replication and supercoiling of Simian virus 40 DNA in cell

- extracts from human cells. *Mol Cell Biol* 1985;5:2051–2060.
39. Berger J, Hauber J, Hauber R, Geiger R, Cullen B. Secreted placental alkaline phosphatase: a powerful new quantitative indicator of gene expression in eukaryotic cells. *Gene*. 1988;66:1–10.
 40. Fallaux FJ, Kranenburg D, Cramer SJ, et al. Characterization of 911: a new helper cell line for the titration and propagation of early region 1-deleted adenoviral vectors. *Hum Gene Ther*. 1996;7:215–222.
 41. Ruffner DE, Stormo GD, Uhlenbeck OC. Sequence requirements of the hammerhead RNA self-cleavage reaction. *Biochemistry*. 1990;29:10595–10702.
 42. Shimayama T, Nishikawa S, Taira K. Generality of the NUX rule: kinetic analysis of the results of systematic mutations in the trinucleotide at the cleavage site of hammerhead ribozymes. *Biochemistry*. 1995;34:3649–3654.
 43. Zoumadakis M, Tabler M. Comparative analysis of cleavage rates after systematic permutation of the NUX↓ consensus target motif for hammerhead ribozymes. *Nucleic Acids Res*. 1995;23:1192–1196.
 44. Homann M, Tabler M, Tzortzakaki S, Sczakiel G. Extension of helix II of an HIV-1 directed hammerhead ribozyme with long antisense flanks does not alter kinetic parameters in vitro but causes loss of the inhibitory potential in living cells. *Nucleic Acids Res*. 1994;22:3951–3957.
 45. Hertel KJ, Herschlag D, Uhlenbeck OC. A kinetic and thermodynamic framework for the hammerhead ribozyme reaction. *Biochemistry*. 1994;33:3374–3385.
 46. Long DM, Uhlenbeck OC. Kinetic characterization of intramolecular and intermolecular hammerhead RNAs with stem II deletions. *Proc Natl Acad Sci U S A*. 1994;91:6977–6981.
 47. Haseloff J, Gerlach WL. Simple RNA enzymes with new and highly specific endoribonuclease activities. *Nature*. 1988;334(6183):585–591.
 48. Persson T, Hartmann RK, Eckstein F. Selection of hammerhead ribozyme variants with low Mg²⁺ requirement: importance of stem-loop II. *Chembiochem*. 2002;3:1066–1071.
 49. Khvorova A, Lescoute A, Westhof E, Jayasena SD. Sequence elements outside the hammerhead ribozyme catalytic core enable intracellular activity. *Nat Struct Biol*. 2003;10:708–712.
 50. Penedo JC, Wilson TJ, Jayasena SD, Khvorova A, Lilley DM. Folding of the natural hammerhead ribozyme is enhanced by interaction of auxiliary elements. *RNA*. 2004;10:880–888.
 51. Canny MD, Jucker FM, Kellogg E, Khvorova A, Jayasena SD, Pardi A. Fast cleavage kinetics of a natural hammerhead ribozyme. *J Am Chem Soc*. 2004;126:10848–10849.
 52. Lilley DM. Ribozymes—a snip too far? *Nat Struct Biol*. 2003;10:672–673.
 53. Carbonell A, Flores R, Gago S. *Trans*-cleaving hammerhead ribozymes with tertiary stabilizing motifs: *in vitro* and *in vivo* activity against a structured viroid RNA. *Nucleic Acids Res*. 2010;39:2432–2444.
 54. Scott WG, Horan LH, Martick M. The hammerhead ribozyme: structure, catalysis and gene regulation. *Prog Mol Biol Transl Sci*. 2013;120:1–23.
 55. De la Pena M, Flores R. An extra nucleotide in the consensus catalytic core of a viroid hammerhead ribozyme: implications for the design of more efficient ribozymes. *J Biol Chem*. 2001;276:34586–34593.
 56. Dufour D, de la Pena M, Gago S, Flores R, Gallego J. Structure-function analysis of the ribozymes of chrysanthemum chlorotic mottle viroid: a loop-loop interaction motif conserved in most natural hammerhead. *Nucleic Acids Res*. 2009;37:368–381.
 57. Shaw LC, Skold A, Wong F, Petters R, Hauswirth WW, Lewin AS. An allele-specific hammerhead ribozyme gene therapy for a porcine model of autosomal dominant retinitis pigmentosa. *Mol Vis*. 2001;7:6–13.
 58. Cideciyan AV, Sudharsan R, Dufour VK, et al. Mutation-independent rhodopsin gene therapy by knockdown and replacement with a single AAV vector. *Proc Natl Acad Sci U S A*. 2018;115:E8547–E8556.
 59. Rosenfeld PJ, Cowley GS, McGee TL, Sandberg MA, Berson EL, Dryja TP. A null mutation in the rhodopsin gene causes rod photoreceptor dysfunction and autosomal recessive retinitis pigmentosa. *Nat Genet*. 1992;1:209–213.
 60. McInnes RR, Bascom RA. Retinal genetics: a nullifying effect for rhodopsin. *Nat Genet*. 1992;1:155–157.
 61. Humphries MM, Rancourt D, Farrar GJ, et al. Retinopathy induced in mice by targeted disruption of the rhodopsin gene. *Nat Genet*. 1997;15:216–219.
 62. Lem J, Krasnoperova NV, Calvert PD, et al. Morphological, physiological, and biochemical changes in rhodopsin knockout mice. *Proc Natl Acad Sci U S A*. 1999;96:736–741.

63. Tan E, Wang Q, Quiamao AB, et al. The relationship between opsin overexpression and photoreceptor degeneration. *Invest Ophthalmol Vis Sci.* 2001;42:589–600.
64. Frederick JM, Krasnoperova NV, Hoffmann K, et al. Mutant rhodopsin transgene expression on a null background. *Invest Ophthalmol Vis Sci.* 2001;42:826–833.
65. Wen XH, Shen L, Brush RS, et al. Overexpression of rhodopsin alters the structure and photo-response of rod photoreceptors. *Biophys J.* 2009;96(3):939–950.
66. Deigan KE, Li TW, Mathews DH, Weeks KM. Accurate SHAPE-directed RNA structure determination. *Proc Natl Acad Sci U S A.* 2009;106:97–102.
67. Du Q, Thonberg H, Wang J, Wahlestedt C, Liang Z. A systematic analysis of the silencing effects of an active siRNA at all single-nucleotide mismatched target sites. *Nucleic Acids Res.* 2005;33:1671–1677.
68. Jackson AL, Burchard J, Schelter J, et al. Widespread siRNA “off-target” transcript silencing mediated by seed region sequence complementarity. *RNA.* 2006;12:1179–1187.
69. Dua P, Yoo JW, Kim S, Lee DK. Modified siRNA structure with a single nucleotide bulge overcomes conventional siRNA-mediated off-target silencing. *Mol Ther.* 2011;19:1676–1687.
70. Kamola PJ, Nakano Y, Takahashi T, Wilson PA, Ui-Tei K. The siRNA non-seed region and its target sequences are auxiliary determinants of off-target effects. *PLoS Comput Biol.* 2015;11:e1004656.
71. Seok H, Lee H, Jang ES, Chi SW. Evaluation and control of miRNA-like off-target repression for RNA interference. *Cell Mol Life Sci.* 2018;75:797–814.
72. Bertrand E, Pictet R, Grange T. Can hammerhead ribozymes be efficient tools to inactivate gene function? *Nucleic Acids Res.* 1994;22:293–300.
73. Emilsson GM, Nakamura S, Roth A, Breaker RR. Ribozyme speed limits. *RNA.* 2003;9:907–918.
74. Breaker RR, Emilsson GM, Lazarev D, et al. A common speed limit for RNA-cleaving ribozymes and deoxyribozymes. *RNA.* 2003;9:949–957.
75. Nelson JA, Uhlenbeck OC. Minimal and extended hammerheads utilize a similar dynamic reaction mechanism for catalysis. *RNA.* 2008;14:43–54.
76. Shepotinovskaya IV, Uhlenbeck OC. Catalytic diversity of extended hammerhead ribozymes. *Biochemistry.* 2008;47:7034–7042.
77. McDowell SE, Jun JM, Walter NG. Long-range tertiary interactions in single hammerhead ribozymes bias motional sampling toward catalytically active conformations. *RNA* 2010;16:2414–2426.